# A model for solar powered aircraft preliminary design

**E. Rizzo and A. Frediani**
University of Pisa
Pisa, Italy

## ABSTRACT

Solar powered aircraft are becoming more and more interesting for future long endurance missions at high altitudes, because they could provide Earth monitoring, telecommunications, etc. without any atmospheric pollution and, hopefully in the near future, with competitive costs compared with satellites. The research activities carried out till now have been mainly focused on flying wings or conventional aircraft configurations, with a great emphasis on the technological aspects. The present paper aims to define a mathematical model for solar powered aircraft preliminary design, valid independently of the aerodynamic configuration. A preliminary analysis is carried out in order to simulate Helios and the results are compared with those available from the flights of this aircraft. The proposed mathematical model is used also to compare four different aircraft configurations, namely: a flying wing, a conventional aircraft, a twin boom aircraft and a biplane aircraft. The results obtained are discussed in the paper and an optimum aircraft is analysed.

## NOMENCLATURE

| | |
|---|---|
| $AM$ | air mass |
| $AR$ | wing aspect ratio |
| $b$ | wingspan |
| $c$ | characteristic length |
| $\bar{c}$ | mean aerodynamic chord |
| $C_f$ | flat plate friction drag coefficient |
| $C_D$, $C_{D0}$, $C_L$ | drag, parasite drag and lift coefficients |
| $C_{Lmax}$ | maximum lift coefficient |
| $E_{flight}$ | required energy for flight |
| $E_{storeIN}$ | input energy to the storage system |
| $E_{storeOUT}$ | output energy from the storage system |
| $E_{sun}$ | solar energy per unit area available inside the atmosphere on a sloped surface |
| $E_{net}$ | net energy for thrust |
| $e$ | Oswald's coefficient |
| $E$ | aerodynamic efficiency $E = L/D$ |
| $E_0$ | solar energy per unit area available outside the atmosphere on a sloped surface |
| $h$ | altitude |
| $h/b$ | height to span ratio |
| $I_0$ | solar power per unit area available, outside the atmosphere |
| $I_{0n}$ | solar power per unit area normal to the surface outside the atmosphere |
| $I_b$ | beam solar power per unit area |
| $I_d$ | diffused solar power per unit area |
| $I_{SC}$ | solar constant |
| $I_{Tot}$ | power per unit area available inside the atmosphere |
| $K = (\pi eAR)^{-1}$ | |
| $L$ | lift or length |
| $n$ | $n$-th day of the year starting from 21 March; load factor |
| $N$ | auxiliary discrete variable defined in the text |
| $NP$ | number of reinforcement bulkheads |
| $p, p_0$ | air pressure at given altitude and air pressure at sea level |
| $P$ | power |
| $P_{flight}$ | required power for flight |

**Paper No. 3184**. Manuscript received 3 October 2006, revised 24 September 2007, accepted 20 December 2007.

https://doi.org/10.1017/S0001924000002001 Published online by Cambridge University Press

$\bar{P}_{flight}$ averaged required power for flight
$P_{net}$ net power for thrust
$R$ cylinder radius
R Reynolds number
$S$ reference area of the generic element, projected onto the horizontal plane
$S^i_b$ wetted area of the $i$-th element
$S^{tot}_b$ total aircraft wetted area
$S^*_c$ area of adjunctive solar panels
$S^i_c$ panelled area of the $i$-th element
$S^{TOT}_c$ total active solar panels area at $AM = 1$
$t/c$ wing thickness to chord ratio
$T$ time period; thrust
$T_d$ diurnal time period
$T_n$ nocturnal time period
$V$ flight speed
$V_z$ flight speed vertical component
$W$ total weight
$W_{af}$ airframe weight
$W_{empty}$ empty weight
$W_{pay}$ payload weight
$W_{prop}$ weight of electric motors
$\alpha$ atmospheric parameter defined in the text; auxiliary function defined in the text
$\alpha_1$ total wetted surface factor defined in the text
$\alpha_i = S^i_b/S_i$ wetted surface factor of the $i$-th surface: ratio of its wetted area to its reference area
$\alpha_s$ solar altitude angle, i.e. the angle between the horizontal plane and the solar beam
$\beta$ angle between the plane containing the surface and the horizon, $0^o \le \beta \le 180^o$; Ångström's turbidity coefficient
$\beta_i$ supplementary factor of the $i$-th element defined in the text
$\gamma$ surface azimuth angle, $-180^o \le \gamma \le 180^o$, 0° indicates South direction, westwards positive; slope of the flight trajectory; extraction factor defined in the text
$\gamma_s$ solar azimuth angle, i.e. the angle on a horizontal surface between the projected solar beam and South direction
$\gamma'_s$ auxiliary angle defined in the text
$\delta$ declination; $-23{\cdot}45^o \le \varphi \le 23{\cdot}45^o$, Northwards positive; fill factor, that is for the $i$-th surface its panelled area to its wetted area ratio $\delta_i = S^i_c/S^i_b$
$\eta$ efficiency, defined in the text
$\eta^*$ global storage system efficiency defined in the text
$\bar{\eta} = \eta\eta^*$
$\eta_{FC}$ fuel cells efficiency
$\eta_m$ electric motors efficiency
$\eta_P$ propeller efficiency
$\eta_{SC}$ solar cells efficiency
$\eta_{Stor}$ storage system efficiency
$(\eta/\rho)_{FC}$ efficiency to density ratio of the fuel cells, motors and
$(\eta/\rho)_{mot}$ solar cells, respectively
$(\eta/\rho)_{SC}$
$\theta$ angle-of-incidence of the beam, i.e. the angle between the beam and the unit vector normal to the surface
$\theta_z$ zenith angle
$\lambda$ wavelength
$\rho$ air density
$\tau_a$ air molecules transmittance coefficient
$\tau_A$ direct radiation transmittance coefficient
$\bar{\tau}_A$ direct radiation average transmittance coefficient
$\tau_{abs}$ absorption transmittance coefficient
$\tau_d$ diffused radiation transmittance coefficient
$\tau_{dust}$ dust transmittance coefficient
$\tau_{Ozone}$ ozone transmittance coefficient
$\tau_{scatt}$ scattering transmittance coefficient
$\tau_w$ falling water transmittance coefficient
$\tau_{Water}$ water vapour transmittance coefficient
$\varphi$ latitude, $-90^o \le \varphi \le 90^o$, Northwards positive
$\omega$ hour angle, due to earth rotation: $\omega = \frac{360}{24} t$ [deg h]
$\omega_{ew}$ auxiliary angle defined in the text

### Subscripts

*b* variable referred to wetted area
*boom* variable referred to the boom
*bulk* variable referred to the bulkhead
*c* variable referred to panelled surfaces
*d* variable referred to diurnal conditions
*fus* variable referred to the fuselage
*Htail* variable referred to the horizontal tail
*min* variable referred to minimum conditions
*max* variable referred to maximum conditions
*n* variable referred to nocturnal or dark conditions
$P_{min}$ variable referred to minimum power condition
*Vtail* variable referred to the vertical tail
*wind* variable referred to maximum wind speed constraint
*wing* variable referred to lifting surfaces

### Superscripts

*alii* variable referred to non lifting surfaces
*c* variable referred to panelled surfaces
*wing* variable referred to lifting surfaces

## 1.0 INTRODUCTION

The use of renewable energy and, in particular, of solar energy, is a challenge of the future. In the aerospace field, a promising future application of the solar energy is the use of high altitude solar powered aircraft (or HALE high altitude long endurance) for telecommunication, surveillance and Earth monitoring[1-4]. The main requirements of a HALE aircraft are to fly at high altitudes (20-30km) for very long missions (some months), and to carry a payload of about 100-300kg. At high altitudes the solar propulsion is attractive because the solar irradiation is intense, air pollution is avoided, and the knowledge and experience on the photovoltaic cells (used during space missions) can be utilised. The long endurance flight is possible when a part of the total solar energy is stored during the day-light in order to fly during the night. The storage energy system can be made of batteries or fuel cells. The weight of the actual batteries per unit of energy is still too big. In the case of fuel cells, a part of the extracted energy is used for water electrolysis producing oxygen and hydrogen that are stored in tanks during the daylight and combined in the fuel cells to produce the electric energy for the nocturnal flight. As a consequence of the large panelled surfaces combined with the necessary high aerodynamic efficiency, HALE aircraft have a very large wingspan and aspect ratio producing high structural deformations in flight and aeroelastic instabilities[5,6]. The most advanced solar aircraft that has been designed up to date was a flying wing, named Helios (NASA and AeroVironment USA) deriving from the previous prototype Pathfinder[7], that crashed on the ground after the installation of the fuel cell system and the storage tanks under the wing in 2003. Even though many problems are to be solved before safe civil applications are possible, the flight of Helios remains the unique demonstration that the solar energy flight is possible at high altitudes. Other activities on solar aircraft have been carried out in Europe[4], even though no flying aircraft has been built till now. The aerodynamic configuration of the European project, named 'Heliplat', is more traditional,

https://doi.org/10.1017/S0001924000002001 Published online by Cambridge University Press

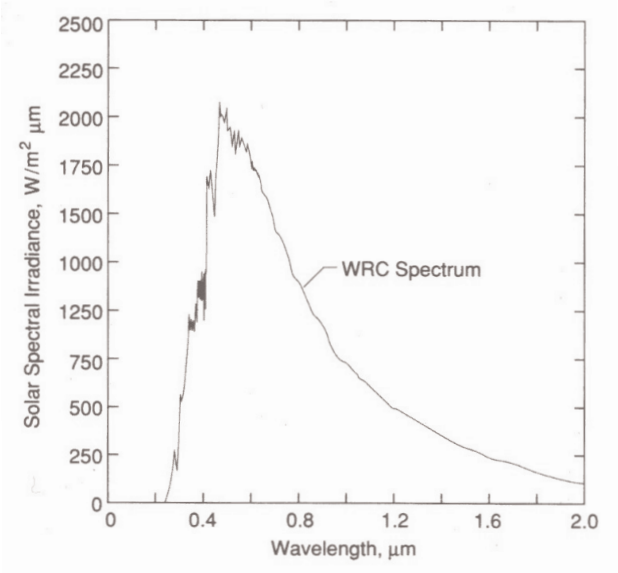



Figure 1. WRC spectrum.

with a wing and a horizontal tail. An open question is whether these two configurations are the results of an optimisation process in which the energetic, aerodynamic, structural, and flight mechanics aspects are taken into account. According to the available literature, the aircraft configuration seems to be designed on the basis of the experience gained before, instead of some optimisation process.

The present paper aims to give a mathematical model for the preliminary design of HALE aircraft. This model is based on the energy balance of a 24 hours horizontal flight (loiter) in a given day of the year, at given latitude and altitude. Any aircraft can be studied and, in this paper, four configurations are analysed, namely: a flying wing, a conventional aircraft, a twin boom and a biplane. In order to check the reliability of the proposed model, the Helios aircraft is simulated and the results are compared with the actual data available from the literature; the obtained results appear to be, in general, reliable. The model is also used to predict the effects of the variations of significant parameters in order to find out the most critical technological parameters of the aircraft. As result, the two configurations named before (USA's Helios and Europe's Heliplat) do not appear as the best possible ones to obtain the maximum endurance flight. All the surfaces of the best solar powered aircraft must be able to generate lift and energy at the same time.

## 2.0 THE SOLAR ENERGY

The available solar energy per unit of area, depends on the atmospheric conditions and on the concentration of atmospheric gases. The first model considered here to predict the amount of energy available, refers to the 'ideal' atmosphere. The atmosphere is treated as a transparent body and, hence, the efficiency of the solar panels is independent of the altitude. Afterwards, the effects of the atmospheric gases, cloudiness, dust, pollutants, etc on the efficiency of the solar panels are taken into account; they depend on the altitude. Most results presented in this section can be found in Ref. 8.

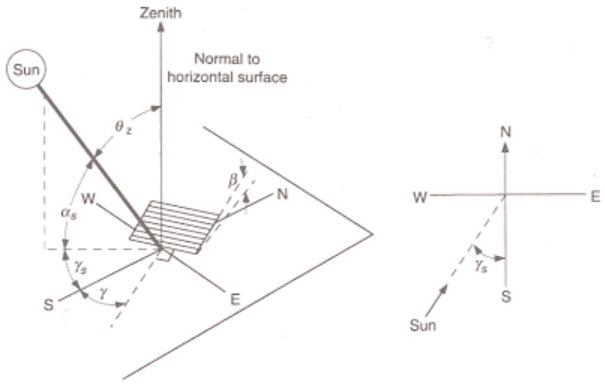



Figure 2. Astronomic angles [from 8].

### 2.1 Solar energy with 'ideal' atmosphere

The radiation emitted by the Sun, outside the Earth atmosphere, is nearly constant and a useful parameter to measure the available solar power is the solar constant ($I_{SC}$), that is the solar power outside the atmosphere per unit time, on a panel of unit area normal to the beam radiation. The World Radiation Center (WRC) has adopted a value of 1,367W/m$^2$ for $I_{SC}$ with an uncertainty of the order of 1%, and has defined the standard spectral irradiance curve shown in Fig. 1. This spectrum is valid in the vacuum (or in the outer space) and this condition is also called air mass zero or AM0.

Under the hypothesis of ideal atmosphere, the power per unit area, on a panel that is normal to the beam radiation, at given latitude and in the $n$th day of the year, $I_{0n}$, depends on the actual position of the Earth along its elliptical trajectory about the Sun. The law of variation in function of the day of the year is given by:

$$I_{0n} = I_{SC}\left(1+0\cdot033\mathrm{Cos}\frac{360n}{365}\right) \quad \ldots (1)$$

If the panel is sloped of the angle $\theta_z$ (see Fig. 2), the solar power per unit area available outside the atmosphere becomes:

$$I_0 = I_{SC}\left(1+0\cdot033\mathrm{Cos}\frac{360n}{365}\right)\mathrm{Cos}\,\theta_z \quad \ldots (2)$$

With reference to Fig. 2, the angle $\theta_z$ depends on the astronomic angles related to the position of the solar panel and on the inclination $\beta$ of the panel on the local horizon.

A significant case is $\beta = 0°$ (the panel belongs to the local horizontal plane). In this case, it can be proved[8] that:

$$\mathrm{Cos}\theta_z = \mathrm{Cos}\varphi\mathrm{Cos}\delta\mathrm{Cos}\omega + \mathrm{Sin}\varphi\mathrm{Sin}\delta \quad \ldots (3)$$

and, by substituting Equation (3) into Equation (2), we get:

$$I_0 = I_{SC}\left(1+0\cdot033\mathrm{Cos}\frac{360n}{365}\right)(\mathrm{Cos}\varphi\mathrm{Cos}\delta\mathrm{Cos}\omega + \mathrm{Sin}\varphi\mathrm{Sin}\delta) \quad \ldots (4)$$

For different values of $\beta$, see Appendix A.

The total solar energy per unit area over a period $T$ is given by integrating the Equation (4) over $T$:

$$E_0 = \int_T I_0 \mathrm{d}t \quad \ldots (5)$$

The available energy depends on the hour in the day, the day in the year, the latitude and the position of the photovoltaic panels.

https://doi.org/10.1017/S0001924000002001 Published online by Cambridge University Press

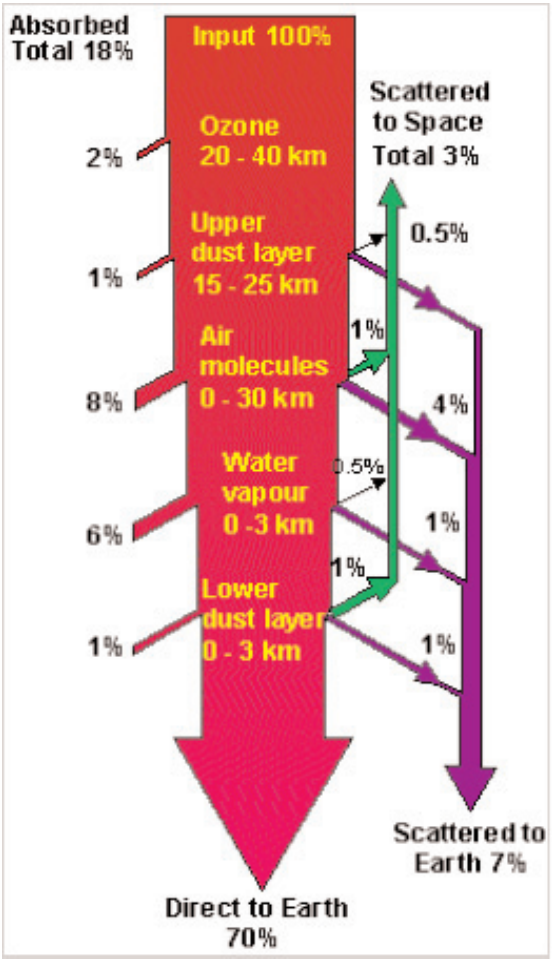



Figure 3. Beam radiation decrement through the atmosphere.

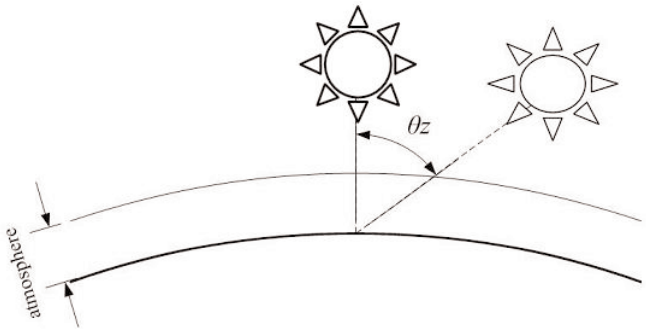



Figure 4. Air mass.

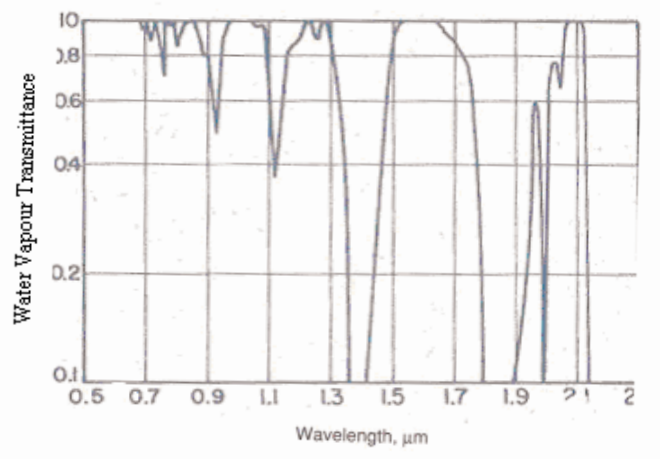



Figure 5. Water vapour absorption spectrum (from Ref. 8).

### 2.2 Available solar energy inside the atmosphere.

When the panels are located inside the atmosphere, other parameters become important as, for example, sky cloudiness, dust concentration, pollutants and altitude; during the passage of the beam radiation through the atmosphere, a part of the radiation is scattered toward space (about 3% of $I_0$), a part is scattered toward the Earth (about 7% of $I_0$), another part is absorbed by the atmospheric gases (about 18% of $I_0$), the rest (70%) constitutes the direct beam radiation (see Fig. 3). The scattering toward outer space is neglected in the present analysis.

To take the above effects into account, a transmittance coefficient for the direct radiation $\tau_A$ and one for the diffused radiation $\tau_d$ are defined. The available solar power at a given altitude is then approximated as:

$$I_{Tot} = I_b + I_d = I_0 \left(\tau_A + \tau_d\right)^{\frac{1}{\mathrm{Cos}\theta_z}} \quad \ldots (6)$$

The term $\frac{1}{\mathrm{Cos}\theta_z}$ is called air mass (AM); it represents the ratio between the real path length of the solar beam and that of minimum distance (see Fig. 4). Due to the Earth's curvature, this definition is valid in the range 0°-70° of $\theta_z$.

A general theory for predicting the diffused radiation is not available; according to Ref. 8, expereriments at low altitudes suggest that the diffused transmittance is much smaller than the direct transmittance and, therefore, we assume $\tau_d = 0$.

The direct or beam transmittance is more significant; it can be divided into two contributions: air scattering and air absorption and, hence, it can be expressed as $\tau_A = \tau_{scatt}(\lambda, h, AM, atm\ cond)\tau_{abs}(\lambda, h, atm\ cond)$.

**Scattering.** Air molecules, dust molecules and water vapour in the atmosphere, produce the phenomenon of scattering and the scattering transmittance can be represented as:

$$\tau_{scatt} = \tau_a \tau_{dust} \tau_w \quad \ldots (7)$$

These terms can be calculated by using either the Rayleigh theory or the Ångström's turbidity equation; more details can be found in Appendix B.

Scattering depends on the air pressure (i.e. on the flight altitude) and on the atmospheric conditions; in particular, it depends on the dust concentration and the water vapour concentration.

**Absorption.** The absorption transmittance is due to the presence of ozone and water vapour, both related to the flight altitude. The ozone

**Table 1**
**Ozone transmittance (from Ref. 8)**

| | | | | | |
|---|---|---|---|---|---|
| $\lambda[\mu m]$ | 0·29 | 0·3 | 0·31 | 0·33 | 0·35 |
| $\tau_{Ozone}$ | 0.0 | 0·1 | 0·5 | 0·9 | 1.0 |

https://doi.org/10.1017/S0001924000002001 Published online by Cambridge University Press

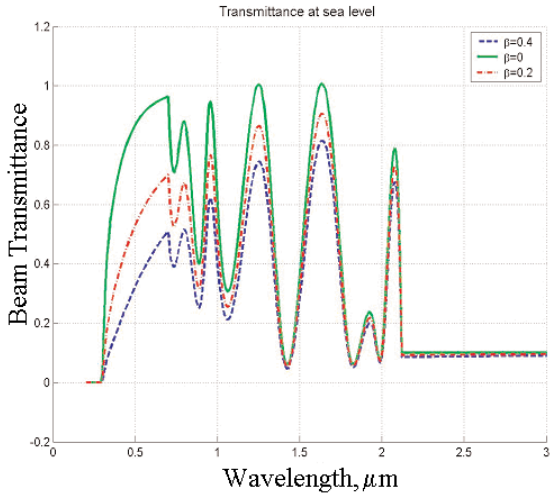



Figure 6. Transmittance at sea level.

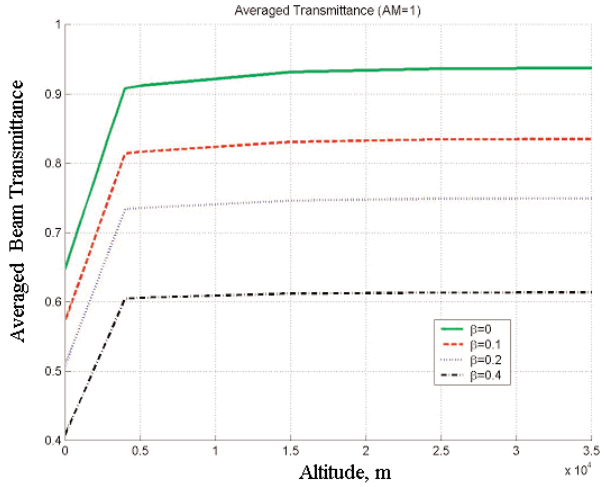



Figure 8. Averaged transmittance.

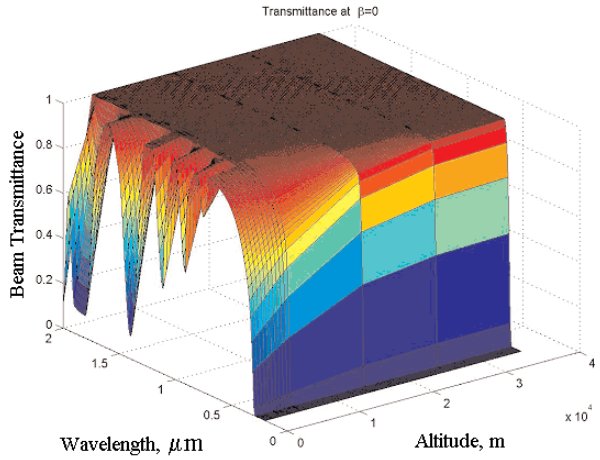



Figure 7. Transmittance versus altitude and wavelength.

absorption is active in the ultraviolet wavelength spectrum, in the range $0{\cdot}29 < \lambda < 0{\cdot}35\ \mu m$, and at high altitudes (20-40km); the ozone transmittance is reported in Table 1.

The water vapour absorption is active in the infrared solar spectrum, close to 1·4 and 1·8 $\mu m$ and only, at low altitudes (0-3 km) (Fig. 5).

At fixed values of the zenith angle and atmospheric conditions, $\tau_A$ depends on the wavelength ($\lambda$) and altitude ($h$).

Figure 6 shows the water vapour transmittance $\tau_A(\lambda)$ for different values of $\beta$, at sea level, with $AM = 1$.

The tri-dimensional plot of the function $\tau_A(\lambda,h)$ for a 'clean sky' condition is shown in Fig. 7. Above the clouds level, $\tau_A(h,\lambda)$ is independent of the wavelength. Below the clouds, because the flight at low altitudes is very short (climb or descent) and in view of engineering applications, we assume and averaged value, $\tau_A(h,\lambda) = \overline{\tau}_A(h)$ where:

$$\overline{\tau}_A(h) = \frac{1}{\lambda_{max} - \lambda_{min}} \int_{\lambda_{min}}^{\lambda_{max}} \tau_A(\lambda, h)\, d\lambda \qquad \ldots (8)$$

The average is performed in the range $\lambda_{min} = 0{\cdot}29\mu m$, $\lambda_{max} = 2{\cdot}5\mu m$. In the Fig. 8 the plots relevant to four different atmospheric conditions (from $\beta = 0$ (clean sky) to $\beta = 0{\cdot}4$ (very turbid sky)) are presented.

Above 3,000m, the averaged transmittance is quite constant and ranges from 0·97 ($\beta = 0$) to 0·6 ($\beta = 0{\cdot}4$). Below 3,000m, the water vapour reduces the transmittance up to 0·66 ($\beta = 0$) and 0·42 ($\beta = 0{\cdot}4$) at sea level.

Once the sky conditions, altitude, latitude, date, hour and solar panel angle are given, the available solar power for unit area can be calculated as:

$$I_{Tot} = I_0 \overline{\tau}_A^{AM} \qquad \ldots (9)$$

where $I_0$ is obtained from Equation (4) and the total available energy in the time period $T$ is given by:

$$E_{sun} = \int_T I_{Tot} S_c^{TOT}\, dt \qquad \ldots (10)$$

where $S_c^{TOT}$ is the total panelled area.

According to this model, the range of the available solar power per unit area, at sea level and $AM = 1$ is $550 \div 1000 W/m^2$.

In order to check the validity of Equation (9), let us compare it with a prediction of the direct solar power given by the following empirical formula valid at sea level:

$$I_b = 1{,}353 \left(0{\cdot}7^{AM}\right)^{0{\cdot}678} \quad \left[Wm^{-2}\right] \qquad \ldots (11)$$

and the total solar power is estimated as:

$$I_{Tot} = 1{\cdot}1 I_b \qquad \ldots (12)$$

with a good agreement between the empirical formula and Equation (9).

## 3.0 ENERGY BALANCE

The energy balance is obtained by imposing the equivalence between the net energy available for the flight ($E_{net}$) and the lost energy due to the aerodynamic drag ($E_{flight}$).

The payload energy is not considered in the present analysis, because it is nearly independent of the flight parameters. Thus, the energy balance becomes, simply:

https://doi.org/10.1017/S0001924000002001 Published online by Cambridge University Press

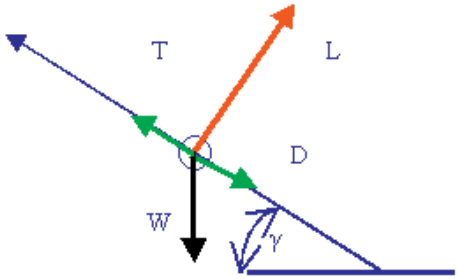



Figure 9. Forces scheme.

$$E_{net} = E_{flight} \quad \ldots (13)$$

The two terms in Equation (13) are now examined separately.

### 3.1 Net solar energy

Let $\eta_P$, $\eta_m$, $\eta_{SC}$ indicate the efficiencies of propellers, electric motors and solar cells, respectively. The global efficiency can be expressed as:

$$\eta = \eta_P, \eta_m, \eta_{SC} \quad \ldots (14)$$

And the net solar power per unit area available for the flight becomes:

$$P_{net} = \eta P_{sum} \quad \ldots (15)$$

The energy, referred to a period $T$ is given by:

$$E_{net} = \int_T \eta I_n S_c^{TOT} \mathrm{d}t \quad \ldots (16)$$

### 3.2 The required energy for flight

As a first approximation, the aircraft is assumed as a material point in steady flight (without taking the stability of flight into account).

With the symbols defined in Fig. 9, the required power for flight becomes:

$$P_{flight} = DV + WV \sin\gamma \quad \ldots (17)$$

Considering small angles of attack and after introducing the lift and drag coefficients $C_L$ and $C_D$ Equation (17) becomes:

$$P_{flight} = WV\left(\frac{C_D}{C_L} + \gamma\right) \quad \ldots (18)$$

and, in terms of energy, we have:

$$E_{flight} = \int_T P_{flight}\,\mathrm{d}t \quad \ldots (19)$$

Different flight strategies can be considered. In the present application of HALE missions, the 'minimum power flight' is assumed as the optimum design criterion.

#### 3.2.1 Minimum power condition

Well-known results from the flight mechanics theory are:

**Minimum power speed:**

$$V_{Pmin} = \frac{V_{Emax}}{\sqrt[4]{3}} \quad \ldots (20)$$

**Minimum power lift coefficient:**

$$C_{LPmin} = \sqrt{3}C_{LPmax} = \sqrt{3C_{D\,0}/K} \quad \ldots (21)$$

where $K$, $S$, $C_{D0}$, $V_{emax}$ are defined in the Nomenclature.

Assuming a parabolic polar curve and, hence, following classical flight mechanics results, the minimum power drag coefficient becomes:

$$C_{DP\,min} = 4C_{D0} \quad \ldots (22)$$

Combining Equation (21) and Equation (22), we have the inverse of the aerodynamic efficiency:

$$\frac{C_D}{C_{L\,P\,\min}} = \frac{4\sqrt{3}}{3}\sqrt{C_{D0}K} \quad \ldots (23)$$

and, from Equation (18), the minimum required power for flight becomes:

$$\begin{aligned} P_{flight}\big|_{min} &= WV_{P\,min}\left.\frac{C_D}{C_L}\right|_{P\,min} + WV_{P\,min}\gamma \\ &= \frac{2^{5/2}}{3^{3/4}}\sqrt{\frac{1}{\rho}}\left(\frac{W}{S}\right)^{3/2} SC_{D0}^{1/4}K^{3/4} + WV_{zP\,min} \end{aligned} \quad \ldots (24)$$

where $V_{zPmin} = V_{Pmin}\gamma$.

We also assume the following limitations on the lift coefficients: to prevent the aerodynamic wing stall,

$$C_L \le C_{Lmax} \qquad \text{to prevent the stall due to front gusts.} \quad \ldots (25)$$

$$C_L \le C_{Lmax}\big|_{wind} = \frac{2W/S}{\rho V_{wind}^2} \quad \ldots (26)$$

The required energy to fly in the period $T$ is:

$$\begin{aligned} E_{flight}\big|_{P\,min} = \int_T P_{flight}\big|_{min}\,dt = \int_T \Bigg[ &\frac{2^{5/2}}{3^{3/4}}\sqrt{\frac{1}{\rho}}\left(\frac{W}{S}\right)^{3/2} SC_{D0}^{1/4}K^{3/4} \\ &+ WV_{zP\,min}\Bigg]\mathrm{d}t \end{aligned} \quad \ldots (27)$$

### 3.3 Energy balance in steady flight.

During one day, a part of the electric energy supplies the steady flight, and another part is stored for the nocturnal flight; we have, then, two conservation energy equations:

$$\begin{cases} E_{sun} = E_{flight}\big|_d + E_{StorIN} \\ E_{StorOUT} = E_{flight}\big|_n \end{cases} \quad \ldots (28)$$

where $E_{storeIN}$ is the energy introduced in the storage system during the daylight and $E_{storeOUT}$ is the energy extracted from it during the night. After introducing the efficiency of the storage system

https://doi.org/10.1017/S0001924000002001 Published online by Cambridge University Press

$$\eta_{Stor} = \frac{E_{StorOUT}}{E_{StorIN}} \quad \ldots (29)$$

the first expression of Equation (28) becomes:

$$E_{sun} = E_{flight}\big| + \frac{E_{flight}\big|_n}{\eta_{Stor}} \quad \ldots (30)$$

and, since

$$E_{flight} = E_{flight}\big|_d + E_{flight}\big|_n$$

Equation (30) becomes:

$$E_{sun} = E_{flight} + E_{flight}\big|_n \left(\frac{1}{\eta_{Stor}} - 1\right) \quad \ldots (31)$$

In a preliminary analysis, the storage system efficiency is supposed to be time independent and long endurance flight (weeks or months) to be performed, hence, the minimum flight duration $T$ is assumed to be one day or:

$$T = T_d + T_n = 24 \text{ hours}, \quad \ldots (32)$$

where $T_d$ and $T_n$ are the hours of daylight and night, respectively (they depend on the day of the year and on latitude).

The energy for a 24-hour flight is given by:

$$E_{flight} = \int_{T_d} P_{flight}\big|_d \, dt + \int_{T_n = 24 - T_d} P_{flight}\big|_n \, dt; \quad \ldots (33)$$

or, equivalently:

$$E_{flight} = \bar{P}_{flight}\big|_d \, T_d + \bar{P}_{flight}\big|_n \, (24 - T_d) \quad \ldots (34)$$

where the averaged values of the diurnal or nocturnal power are introduced.

Under the hypothesis that the averaged required power to fly is independent of day and night aircraft flight, or:

$$\bar{P}_{flight}\big|_d = \bar{P}_{flight}\big|_n = \bar{P}_{flight}$$

Equation (34) can be written as:

$$E_{flight} = 24 \bar{P}_{flight} \quad \ldots (35)$$

and Equation (31) becomes:

$$E_{sun} = E_{flight} + \frac{T_n}{24} E_{flight} \left(\frac{1}{\eta_{Stor}} - 1\right) = E_{flight} \left[1 + \frac{T_n}{24}\left(\frac{1}{\eta_{Stor}} - 1\right)\right] \quad \ldots (36)$$

The term $\left[1 + \frac{T_n}{24}\left(\frac{1}{\eta_{Stor}} - 1\right)\right]$ (>1) is the inverse of an efficiency,

depending on $T_n$ and $\eta_{Stor}$.

By defining the global efficiency of the storage system as:

$$\eta^* = \frac{1}{\left[1 + \frac{T_n}{24}\left(\frac{1}{\eta_{Stor}} - 1\right)\right]} \quad \ldots (37)$$

we have:

$$\eta^* E_{sun} = E_{flight} \quad \ldots (38)$$

and the general expression of energy balance in steady flight becomes:

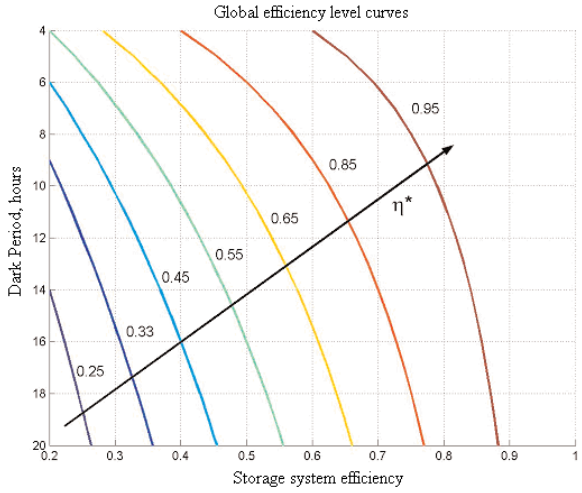



Figure 10. $\eta^*$ level curves plot.

$$\int_{T_d} \eta\eta^* I_n S_C^{TOT} dt = \int_T \left[\frac{2^{5/2}}{3^{3/4}} \sqrt{1/\rho} \, (W/S)^{3/2} \, S C_{D0}^{1/4} K^{3/4} + W V_{zPmin}\right] dt \quad \ldots (39)$$

In particular, in the case of horizontal flight, Equation (39) becomes:

$$\int_{T_d} \eta\eta^* I_n S_C^{TOT} dt = \int_T \left[\frac{2^{5/2}}{3^{3/4}} \sqrt{1/\rho} \, (W/S)^{3/2} \, S C_{D0}^{1/4} K^{3/4}\right] dt \quad \ldots (40)$$

Figure 10 shows some contour lines of $\eta^*$ *versus* the nighttime duration $T_n$, for a set of energy storage efficiencies. If, for example, $\eta_{Stor} = 0{\cdot}5$, we have $\eta^* = 0{\cdot}8$ in summer (i.e. eight hours night time), while in winter (i.e. 16 hours night time) $\eta^* = 0{\cdot}55$. If one wishes to have global efficiency $\eta^* = 0{\cdot}85$ during the whole year (from eight up to 16 hours of night), the storage system efficiency must improve from $\eta_{Stor} = 0{\cdot}58$ to $\eta_{Stor} = 0{\cdot}72$ (at medium latitudes of reference).

Now the energy balance equation has to be properly modified, when the lift limitations (25) and (26) occur.

CASE 1. $C_L = C_{Lmax}$.

In the case of maximum lift coefficient to prevent the wing stall, the flight speed is given by:

$$V_{C_{L\,max}} = \sqrt{\frac{2W/S}{\rho C_{L\,max}}} \quad \ldots (41)$$

Therefore, the flight power is:

$$P_{flight}\big|_{C_{Lmax}} = W \sqrt{\frac{2W/S}{\rho C_{Lmax}}} \left(\frac{C_{D0} + K C_{Lmax}^2}{C_{Lmax}} + V_{ZC_{Lmax}}\right) \quad \ldots (42)$$

from which the general energy balance equation becomes:

$$\int_{T_d} \eta\eta^* I_n S_C^{TOT} dt = \int_T \left[\sqrt{2/\rho} \, (W/S)^{3/2} \frac{C_{D0} + K C_{Lmax}^2}{C_{Lmax}^{3/2}} S + W V_{zC_{Lmax}}\right] dt \quad \ldots (43)$$

and in horizontal flight ($V_z = 0$):

$$\int_{T_d} \eta\eta^* I_n S_C^{TOT} dt = \int_T \left[\sqrt{2/\rho} \, (W/S)^{3/2} \frac{C_{D0} + K C_{Lmax}^2}{C_{Lmax}^{3/2}} S\right] dt \quad \ldots (44)$$

https://doi.org/10.1017/S0001924000002001 Published online by Cambridge University Press

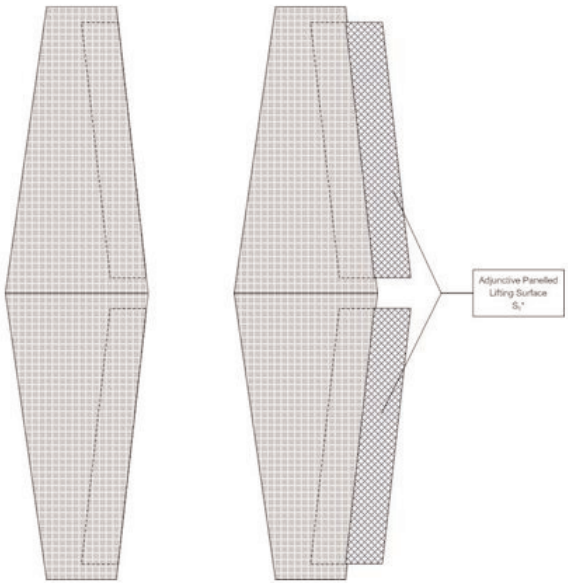



Figure 11. Panelled wing (left) and panelled wing with adjunctive panelled lifting surfaces (right).

CASE 2. $C_L \le C_{L_{max}}\big|_{wind}$

In this case we put $V = V_{max}\big|_{wind} = V_{wind}$ and the lift coefficient becomes:

$$C_{Lwind} = \frac{2W/S}{\rho V_{wind}^2} \qquad \ldots (45)$$

so, the flight power is:

$$P_{flight}\big|_{maxwind} = \frac{\rho C_{D0} V_{wind}^3}{2} S + 2\frac{K}{\rho V_{wind}}\left(\frac{W}{S}\right)^2 S + WV_{zwind} \qquad \ldots (46)$$

and the energy balance equation becomes:

$$\int_{T_d} \eta\eta^* I_n S_C^{TOT} \mathrm{d}t = \int_T \left[\frac{S}{2}\rho C_{D0} V_{wind}^3 + 2\left(W/S\right)^2 K \frac{S}{\rho V_{wind}} + WV_{zwind}\right]\mathrm{d}t \qquad \ldots (47)$$

In the case of horizontal flight, $\gamma = 0$ and Equation (47) is simplified in:

$$\int_{T_d} \eta\eta^* I_n S_C^{TOT} \mathrm{d}t = \int_T \left[\frac{S}{2}\rho C_{D0} V_{wind}^3 + 2\left(W/S\right)^2 K \frac{S}{\rho V_{wind}}\right]\mathrm{d}t \qquad \ldots (48)$$

When the balance Equations (43) and (48) are satisfied, the continuous 24-hour solar powered flight is possible.

## 4.0 SOME DEFINITIONS ON PHOTO VOLTAIC PANELS

Aircraft configurations are defined by means of some geometric parameters, which are analysed in this section.

**Whole aircraft wetted surface, $S_b^{TOT}$**

The quantity $S_b^{TOT}$ is the total wetted surface, both lifting and non-lifting referred to the reference surface $S_{wing}$. For example, in a flying wing, if $S_{wing}$ indicates the wing surface (or reference surface), the whole wetted area is $S_b^{TOT} = 2S_{wing}$. A general expression used in this paper is the following:

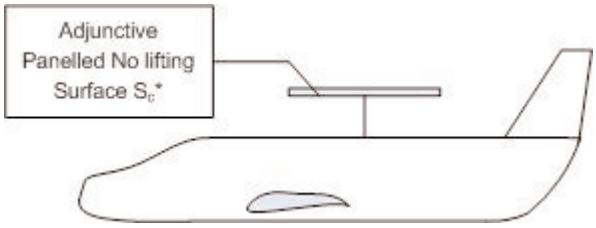



Figure 12. Example of adjunctive panelled no-lifting surfaces.

**Table 2**
**Geometric values for the flat panel**

| | $S_{ref}$ | $S_b$ | $S_c$ | $\alpha_w$ | $\delta$ |
|---|---|---|---|---|---|
| Mode 1 | $S$ | $2S$ | 0 | 2 | 0 |
| Mode 2 | $S$ | $2S$ | $S$ | 2 | 0·5 |

$$S_b^{TOT} = S_{wing} \sum_i \alpha_i \beta_i \qquad \ldots (49)$$

where: $\beta_i = \begin{cases} 1 & \text{for the lifting surfaces} \\ \gamma_C & \text{for the extra panelled surfaces} \\ \beta_i & \text{for all the other surfaces} \end{cases}$

$\alpha_i \ge 2$

$\gamma_C = \dfrac{S_C{}^*}{S_{wing}}$ or 'extraction factor' indicates the panelled surface ($S_C^*$) added during the mission, in general: $\gamma_c = \gamma_c(t)$ (see Figs 11 and 12);

$\beta_i = \dfrac{S_{alii}}{S}$ or 'supplementary factor' indicates the percentage of non lifting surface ($S_{alii}$) of the aircraft respect to the reference surface; $\beta_i > 0$.

**Active panelled surface:**

The active panelled surface is the part of the wetted surface covered with active solar panels, at time $t$. If this part is indicated with $\delta_i$, the active panelled surface $S_c^{TOT}$ becomes (the symbols are defined in the Nomenclature):

$$S_e^{TOT} = S_{wing} \sum_i \delta_i \alpha_i \beta_i \qquad \ldots (50)$$

where: $\delta_i = \delta_i < (t)$ 1 (if $\delta_i = 0$, the surface has no active panel).

In order to write Equations (49) and (50) in a compact form, we define the 'alpha function' as:

$$\alpha(\delta) = \sum_i \delta_i \alpha_i \beta_i \qquad \ldots (51)$$

hence the following compact definitions hold:

$$\begin{aligned} S_e^{TOT} &= S_{wing}\,\alpha \\ S_b^{TOT} &= S_{wing}\,\alpha\big|_{\delta=1} = S_{wing}\,\alpha_t \end{aligned} \qquad \ldots (52)$$

The symbol $\alpha_t = \alpha\big|_{\delta=1}$, called 'total wetted surface factor', is the whole wetted area to the wing (reference) area ratio.

High values of $\alpha/\alpha_1 = S_c^{TOT}/S_{wing}$ indicate that the most part of the wing is covered with photovoltaic panels. The ratio $\alpha = S_c^{TOT}/S_b^{TOT}$ is used to compare different solutions (the optimum is $\alpha/\alpha_1 = 1$).

Figure 13 shows a flat panel with photovoltaic cells on top and

https://doi.org/10.1017/S0001924000002001 Published online by Cambridge University Press

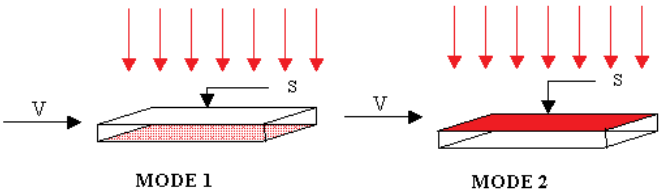



Figure 13. Flat panel geometry.

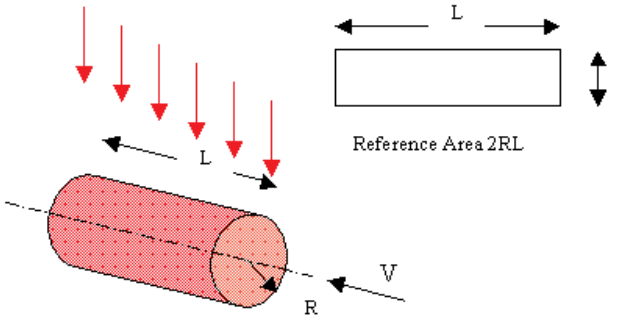



Figure 14. Cylinder with horizontal axis.



Figure 15. Flying wing configuration.

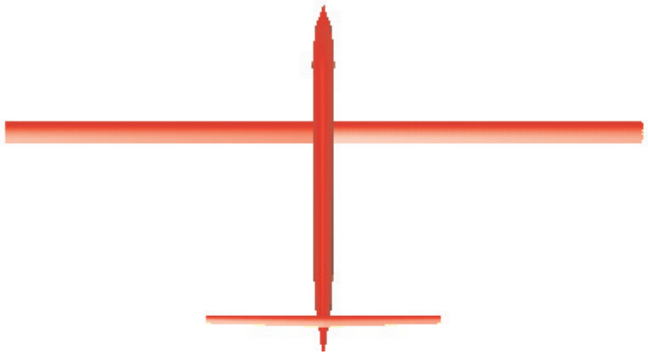


Figure 16. Conventional architecture.



Figure 17. Twin boom architecture.

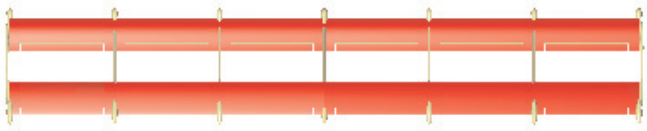


Figure 18. Biplane architecture.

**Table 3**
**Geometric values for the cylinder**

| | $S_{ref}$ | $S_b$ | $S_c$ | α | δ |
|---|---|---|---|---|---|
| Cylinder | $2RL$ | $2\pi RL$ | $2RL$ | π | $1/\pi$ |

bottom faces (mode 1 and mode 2) referred to irradiation; the values of the geometric parameters are also reported in Table 2.

A circular cylinder with the horizontal axis, covered with cells on the whole external surface, is shown in Fig. 14. The geometric parameters are reported in Table 3.

By means of these two basic geometries, it is possible to investigate the effect on the balance equations of many aircraft configurations. In this paper, four different configurations are examined and the relevant geometric parameters are collected in Table 4. The aerodynamic surfaces are supposed to be flat panels, and the fuselage is assumed as a circular horizontal cylinder.

In Fig. 15 a flying wing is shown; this solution is the closest one to NASA prototypes.

Figure 14 shows a conventional architecture made of a wing, a fuselage and a tail. A conventional architecture with twin boom (to substitute the conventional fuselage) is shown in Fig. 17.

Finally, Fig. 18 shows a biplane configuration, with intermediate reinforcement bulkheads. The bulkheads permit the load transfer between the two wings, belonging to two different and parallel levels; the front wing is lower and the rear one is higher. At each bulkhead station, a pair of electric motors are installed, one for each wing, as shown more clearly later on.

The energetic efficiency of the configurations is quantified by the $\alpha/\alpha_1$ ratio; Table 4 shows that the flying wing is the best solution from the energetic and aerodynamic viewpoints, even though the structural efficiency is a critical aspect. The flights of the flying wing Helios in 2003 showed large bending and torsional deformations, and this reduced efficiency of aerodynamic controls; the flying wing became unstable in flight and crashed on the ground. In conclusion, even though the flying wing is the best solution from an aerodynamic and energetic point of view, the structural efficiency plays a fundamental role in the HALE aircraft[9,10] so that the structural weight improvement reduces the global efficiency of the configuration. Similar problems are supposed to be present in the case of conventional configurations with a classic cantilever wing; in this case the energy efficiency is lower than the flying wing's one.

The reinforced biplane structure has been conceived in order to avoid structural problems. This solution demonstrates a high aerodynamic and energetic efficiency, and the airframe weight is also about 80% of the flying wing. More details will be given later on.

## 5.0 AIRCRAFT DESIGN PROCEDURE

The previous energy balance equations are valid for any kind of missions. The same equations can be simplified in the hypothesis of loiter at constant altitude or:

- $\rho = \text{const}$
- $V_z = 0$

We assume also that the parasite drag coefficient can be predicted by the flat plate analogy. Equations (54) and (55) are the simplest model for the prediction of the friction drag coefficient :

$$C_{D0} = C_f \frac{S_b^{TOT}}{S} \qquad \ldots (53)$$

$$C_f = \frac{1{\cdot}328}{\sqrt{\mathrm{Re}}} \text{ for } \mathrm{Re} \le 485{,}000 \text{ (Laminar flow);} \qquad \ldots (54)$$

https://doi.org/10.1017/S0001924000002001 Published online by Cambridge University Press

**Table 4**
**Different geometrical data. More details are given in Appendix C**

| | Conventional | Twin boom | Flying wing | Biplane |
|---|---|---|---|---|
| $S_{ref}$ | $S_{wing}$ | $S_{wing}$ | $S_{wing}$ | $S_{wing}$ |
| $S_{alii}$ | $S_{fus}$<br>$S_{Htail}$<br>$S_{Vtail}$ | $S_{boom}$<br>$S_{Htail}$<br>$S_{Vtail}$ | $S_{pod}$ | $S_{bulk}$ |
| β | $\beta_{fus} \approx R/c$<br>$\beta_{Htail} \approx 4/AR$<br>$\beta_{Vtail} \approx 0{\cdot}036/AR_{VT}$<br>$\beta_{pod} = \frac{(t/c)_{pod}}{AR}$ | $\beta_{boom} \approx 2R/c$<br>$\beta_{Htail} \approx 0{\cdot}31$<br>$\beta_{Vtail} = 0{\cdot}1\frac{(t/c)_{VT}}{AR_{VT}}$<br>$\beta_{pod} = \frac{(t/c)_{pod}}{AR}$ | $\beta_{pod} = \frac{(t/c)_{pod}}{AR}$ | $_{bulk} \approx 0{\cdot}2/AR_{wing}$ |
| $\alpha_i$ | $\alpha_{wing} \approx 2$<br>$\alpha_{Htail} \approx 2$<br>$\alpha_{VT} = \frac{AR_{VT}}{(t/c)_{VT}}$ | $\alpha_{wing} \approx 2$<br>$\alpha_{Htail} \approx 2$<br>$\alpha_{VT} = 2\frac{AR_{VT}}{(t/c)_{VT}}$ | $\alpha_{wing} \approx 2$<br>$\alpha_{pod} \approx 1/(t/c)_{pod}$ | $\alpha_{wing} \approx 2$<br>$\alpha_{bulks} \approx 10\ AR_b = 10\ h/b$ |
| π | $\alpha_{fus} \approx \pi$<br>$\alpha_{pod} \approx 1/(t/c)_{pod}$ | $\alpha_{booms} \approx \pi$<br>$\alpha_{pod} \approx 1/(t/c)_{pod}$ | | $AR_{wing}$ |
| δ | $\delta_{wing} = ½$<br>$\delta_{Htail} = ½$<br>$\delta_{Vtail} = 0$<br>$\delta_{fus} = 1/\pi$<br>$\delta_{pod} = 0$ | $\delta_{wing} = ½$<br>$\delta_{Htail} = ½$<br>$\delta_{Vtail} = 0$<br>$\delta_{boom} = 0$<br>$\delta_{pod} = 0$ | $\delta_{wing} = ½$<br>$\delta_{pod} = 0$ | $\delta_{wing} = ½$<br>$\delta_{bulk} = ½$ |
| α | $\approx 1 + 4/AR + R/c$ | 1·31 | $\alpha \approx 1$ | $\alpha \approx 1$ |
| $\alpha_1$ | $\approx 2{\cdot}16 + 8/AR + 0{\cdot}72 + \pi R/c$ | $2{\cdot}98 + 2\pi R/c$ | $\alpha_1 = 2{\cdot}16$ | $2 + 10\ h/b\ AR_{wing}\ NP\ \beta_{bulk}$ |
| $S_b^{TOT}$ | $S_{wing}(2{\cdot}16 + 8/AR + 0{\cdot}72 + \pi R/c + \alpha_c\gamma)$ | $S_{wing}(2{\cdot}98 + 2\pi R/c + \alpha_c\gamma)$ | $S_{wing}(2{\cdot}16 + \alpha_c\gamma)$ | $\approx S_{wing}(2\ (1 + h/b\ NP) + \alpha_c\gamma)$ |
| $S_c^{TOT}$ | $S_{wing}(1 + 4/AR + R/c + \delta_c\alpha_c\gamma)$ | $S_{wing}(1{\cdot}31 + \delta_c\alpha_c\gamma)$ | $S_{wing}(1 + \delta_c\alpha_c\gamma)$ | $S_{wing}(1 + \delta_c\alpha_c\gamma)$ |
| $\alpha/\alpha_1$ | $\frac{1 + 4/AR + R/c}{2{\cdot}88 + 8/AR + \pi R/c} \approx 0{\cdot}35$ | $\frac{1{\cdot}31}{2{\cdot}98 + 2\pi R/c} \approx 0{\cdot}38$ | 0·46 | $\frac{1}{2 + 2h/bNP} \approx 0{\cdot}38 \div 0{\cdot}4$ |

$$C_f = \frac{0{\cdot}074}{\sqrt[5]{\mathrm{Re}}} - \frac{1{,}700}{\mathrm{Re}} \text{ for Re} > 485{,}000 \text{ (Turbulent flow).} \quad \ldots (55)$$

The energy balance equations become:

**Minimum Power energy balance:**

$$\int_{T_d} \eta\eta^* I_{Tot} S_c^{TOT} \mathrm{d}t = 2^{5/2}/3^{3/4}\,\rho^{-1/2} \left\{ \int_{T_d} \left[ (W/S_d)^{3/2} C_f^{1/4} (\pi eAR)^{-3/4} S_d \left(S_b^{TOT}/S\right)_d \right] \mathrm{d}t + \right.$$

$$\left. + \int_{T_n = 24 - T_d} \left[ (W/S_n)^{3/2} C_f^{1/4} (\pi eAR)^{-3/4} S_n \left(S_b^{TOT}/S\right)_n \right] \mathrm{d}t \right\} \quad \ldots (56)$$

**Minimum Power energy balance with constraint on the maximum lift coefficient:**

$$\int_{T_d} \eta\eta^* I_{Tot} S_c^{TOT} \mathrm{d}t = \sqrt{2}\rho^{-1/2} \left\{ \int_{T_d} \left[ (W/S_d)^{3/2} \left(C_f S_b^{TOT}/S\right)_d S_d / C_{Lmax}^{3/2} + C_{Lmax}^2/\pi eAR \right] \mathrm{d}t + \right.$$

$$\left. + \int_{T_n = 24 - T_d} \left[ (W/S_n)^{3/2} \left(C_f S_b^{TOT}/S\right)_n S_n / C_{Lmax}^{3/2} + C_{Lmax}^2/\pi eAR \right] \mathrm{d}t \right\} \quad \ldots (57)$$

**Minimum Power energy balance with constraint on the maximum wind speed:**

$$\int_{T_d} \eta\eta^* I_{Tot} S_c^{TOT} \mathrm{d}t = \int_{T_d} \left[ \rho/2 \left(C_f V_{wind}^3 S_b^{TOT}/S\right)_d S_d + 2/\rho \left(\pi eAR V_{wind}\right)_d^{-1} (W/S_d)^2 S_d \right] \mathrm{d}t + \quad \ldots (58)$$

https://doi.org/10.1017/S0001924000002001 Published online by Cambridge University Press

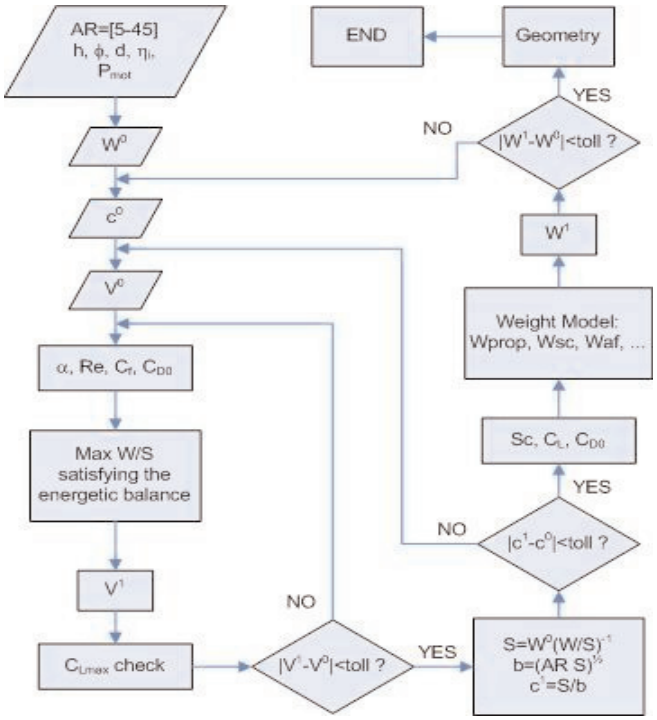



Figure 19. Flow chart of the iterative solution.

$$+\int_{T_n=24-T_d}\left[\rho/2\left(C_f V_{wind}^3 S_b^{TOT}/S\right)_n S_n + 2/\rho\left(\pi eAR V_{wind}\right)_n^{-1}\left(W/S_n\right)^2 S_n\right]dt$$

The reference area $S$ (or $S_n$ or $S_d$) is the area of all the positive lifting surfaces, i.e. the wing(s), the adjunctive panelled lifting surfaces $S_c^*$, or any other surface producing an upward aerodynamic force, (e.g. the tail surface in trimmed flight is not accounted for, when it produces a negative (downward) lift). Therefore the reference area can be expressed as:

$$S = S_{wing} + S_C^* = S_{wing}\left(1+\gamma_C\right)^N \quad \ldots (59)$$

where $N = 0$, if the adjunctive surfaces are non-lifting or negative lifting, and $N = 1$ if the adjunctive surfaces are (positive) lifting.

The Reynolds number, Re, is a function of a reference length (for example the mean aerodynamic chord, still unknown), of the kinematic viscosity ($v$), flight speed ($V$), and, hence, the previous Equation (56) with the constraint (57) and (58) can be solved only iteratively. The flow chart for the mathematical solution is shown in Fig. 19.

After the introduction of the parameter , the three Equations (56), (57) and (58) are simplified; further simplifications follow from the following hypotheses:

- $\alpha(t)$ = const
- $C_f$ , e, $AR$ = 0 are constant in the time interval considered;
- $\gamma_d = \gamma_n = \gamma$ (or: the adjunctive panels during the day and the night are the same);
- $V$ = const;

Under these hypotheses the previous equations become:

**Minimum Power energy balance:**

$$\int_{T_d}\eta\eta^* I_{Tot}dt = 2^{5/2}/3^{3/4}\rho^{-1/2}\left(W/S_{wing}\right)^{3/2} C_f^{1/4}\left(\pi eAR\right)^{-3/4} \quad \ldots (60)$$

$$\left(1+\gamma_C\right)^{-N/2} 24\,\alpha_1\left(\gamma_C\right)/\alpha\left(\gamma_C\right)$$

**Minimum Power energy balance with constraint on the maximum lift coefficient:**

$$\int_{T_d}\eta\eta^* I_{Tot}dt = \sqrt{2}\rho^{-1/2}\left(W/S_{wing}\right)^{3/2} 24\,\frac{C_f\alpha_1\left(\gamma_C\right)+C_{Lmax}^2/\pi eAR}{\alpha\left(\gamma_C\right)C_{Lmax}^{3/2}\left(1+\gamma_C\right)^{N/2}} \quad \ldots (61)$$

**Minimum Power energy balance with constraint on the maximum wind speed:**

$$\int_{T_d}\eta\eta^* I_{Tot}dt = 24/\alpha\left(\gamma_C\right)\left[\rho/2\,C_f V_{wind}^3\alpha_1\left(1+\gamma_C\right)^N + 2/\rho\left(W/S_{wing}\right)^2\left(\pi eAR V_{wind}\right)^{-1}\left(1+\gamma_C\right)^{-N}\right] \quad \ldots (62)$$

By means of these equations, it is possible to calculate the cruise speed using the iterative procedure shown in Fig. 19, consisting of the following steps:

1. Set a starting weight $W_0$
2. Set a starting mean aerodynamic chord $\bar{c}_0$.
3. Set a starting speed $V_0$.
4. Calculate the Reynolds number.
5. Obtain the maximum wing loading allowable to accomplish the 24 hours mission at minimum power condition, namely:

$$\left(\frac{W}{S_{wing}}\right)_{Pmin} = \left[\frac{\int_{T_d}\eta\eta^* I_{Tot}dt}{2^{5/2}/3^{3/4}\rho^{-1/2}\left(W/S_{wing}\right)^{3/2} C_f^{1/4}\left(\pi eAR\right)^{-3/4}\left(1+\gamma_C\right)^{-N/2}24\,\alpha_1\left(\gamma_C\right)/\alpha\left(\gamma_C\right)}\right]^{2/3} \quad \ldots (63)$$

6. $V_{Pmin}$ is then obtained and the new Reynolds number and can be calculated:

$$C_{LPmin} = \sqrt{\frac{3C_{D0}}{K}} \quad \ldots (64)$$

with two possible cases:

(a) If $C_{Lmin} \geq C_{Lmax}$ then, $C_L = C_{Lmax}$, $C_D = C_{D0} + KC_L^2$ and, after (41)

$$V_{C_{Lmax}} = \sqrt{\frac{2W/S}{\rho C_L}}$$

(b) If $V_{Pmin} \leq V_{wind}$ or $V_{CLmax} \leq V_{wind}$, then set $V = V_{wind}$ and the maximum wing loading is obtained.

7. Update $V$ and go to 3. until convergence.
8. Once the wing loading is obtained, the wing area is given by:

$$S_{wing} = W\left(\frac{W}{S_{wing}}\right)^{-1} \quad \ldots (65)$$

(the weight model is presented later on).

9. Given the aspect ratio AR, the wingspan is known:

$$b = \sqrt{S_{wing}AR} \quad \ldots (66)$$

10. Assuming a rectangular wing, the mean aerodynamic chord is:

$$\bar{c} = \frac{S_{wing}}{b} \quad \ldots (67)$$

https://doi.org/10.1017/S0001924000002001 Published online by Cambridge University Press

**Table 5**
**Different solar cells efficiencies**

| Solar cell | ρ[kg/m²] | η | ρ/η[kg/m²] |
|---|---|---|---|
| Si[1] | 0·3651 | 19% | 1·89 |
| AsGa 3 junction | 1·325 | 28-30% | 4·65 |
| AsGa 1 junction | 0·7 | 21% | 3·33 |

**Table 6**
**Fuel cells storage system data**

| Item | Specific power or specific energy or weight |
|---|---|
| Fuel cells | 650W/kg |
| Reactants | 2·6kW/kg |
| Tank | 3·4kW/kg |
| Storage system | 2 kWh/kg |
| Compressor at 3·5bar | 40kg |
| System batteries | 0·3% flight energy |

**Table 7**
**Mission data and components' efficiencies**

| Item | Value |
|---|---|
| Latitude | 14 °N |
| Date | 25/06 |
| Altitude | 30km |
| Payload | 300kg |
| Silicon solar cells efficiency | η = 0·19 |
| Brushless electric motors efficiency | η = 0·85 |
| High altitude optimised propeller efficiency | η = 0·8 |
| Fuel cells efficiency | η = 0·5 |
| Panelled Area/wing area | 0·8 |
| $V_{wind}$ | 50ms$^{-1}$ |
| Max lift coefficient allowed $C_{Lmax}$ | 1 |

11. Update the chord and go to 2. until convergence.
12. The wing is fully defined and, hence, it is possible to calculate its weight and the weights of the components together with lift, drag and required power to fly. Update the weight and go to 1. until convergence.

This procedure is performed for a fixed aspect ratio and, hence, we have a set of solutions depending on $AR$. It is clear that the most convenient strategy in adding panelled surfaces, is to use lifting panelled surfaces (i.e. $N = 1$) because, in this case, the right hand side of Equation (60) grows as $\gamma_C^{N/2}$, hence, a lower solar energy is required (or more payload is available) to balance the equation.

## 6.0 EMPTY WEIGHT PREDICTION MODEL

For solar powered aircraft, it is difficult to define a good structural weight model, because too few data are available or too few flying aircraft have been manufactured (the NASA prototypes Pathfinder, Centurion, Helios).

In this paper, two kind of predictions are adopted; the first one is based on statistical data for sailplanes with twin boom[1], whilst the second is obtained by interpolating the data published for the NASA prototypes.

The first weight model (to be preferred for manned vehicles) is the following:

$$W_{af} = 0{\cdot}31 n^{0{\cdot}311} S^{0{\cdot}778} AR^{0{\cdot}417} \quad [W\text{: lb; S: ft}^2] \qquad \ldots (68)$$

For the second model (to be preferred for UAV) we get the following equation:

$$W_{af} = 1{\cdot}548 S^{0{\cdot}656} AR^{0{\cdot}6514} \quad [W\text{: kg; S: m}^2] \qquad . (69)$$

These models could give reasonable weight estimations for conventional or twin-boom aircraft but not in the case of biplane or multiplane configurations. The structure of a biplane examined here is over-constrained due to the vertical structures between the upper and lower wings; a preliminary analysis indicates that the weight for a biplane is about 80% of the flying wing weight.

**Solar cells weight estimation**

Weight and efficiency of the solar cells are the main parameters for the HALE aircraft design. The solar cells considered in this paper are listed in Table 5, together with their values of ρ, η, ρ/η.

The solar cells must be provided with a coolant system, whose weight is estimated as 20% of the cell weight, to be added to the values in Table 5.

**Storage system weight estimation**

The storage energy system considered here is a fuel cell plant, made of a fuel cell package, a hydrogen storage tank, a hydrogen storage-electrolyser system, a reactant ($H_2$) and a compressor. Weight data referred to today technology are shown in Table 6.

The fuel cell system is the most efficient storage system available today in terms of weight to power ratio. In fact, if batteries substitute fuel cells, the specific energy becomes 35Wh/kg (for PbA batteries) and 100Wh/kg (Li-Ion batteries).

**Electric Motors weight estimation**

The data reported below refer to commercial brushless electric motors of the present generation; a linear approximation of the weight function versus the required power for the propulsion, is given by:

$$W_{prop} = 0{\cdot}0045 P_{prop} \qquad (W \text{ in [kg], P in watts}) \qquad \ldots (70)$$

In the design process, an increase of 20% of the required power is considered in order to take the take-off phase into account[4].

## 7.0 VALIDATION OF THE MATHEMATICAL MODEL

In order to validate the proposed mathematical model, calculations are performed with reference to a flying wing and compared to the data of Helios aircraft[5].

The Helios prototype was designed to fly at 24km of altitude with a payload of 330kg (600lb) to demonstrate an endurance target of 48 hours continuum flight, or at 30km with a payload of 55kg (100lb) (altitude target); the reference flight date is 25 June, at the latitude of the Hawaii Islands.

The technical data of the components and the reference conditions for the validation are shown in Table 7.

Some comparisons are shown in Figs 18-20. The number of hours refers to the flight hours after the sunset (from 2 to 10h), whereas the 24 hours refers to one-day flight. As said before, the model predictions refer to the optimum long endurance design condition.

Figure 18 shows that the Helios wingspan is lower than that predicted by the model in the optimum long endurance flight condition; hence, Helios wingspan seems to be underestimated.

Moreover, the empty weight comparison is reported with two different mission profiles, namely: loiter at maximum altitude of 30,000m and with no nocturnal flight, and loiter at 20,000m in maximum endurance condition, i.e. daily and nocturnal flight; the results predicted are comparable with the Helios empty weight.

Figure 19 refers to wing loading and wing area; the predicted

https://doi.org/10.1017/S0001924000002001 Published online by Cambridge University Press

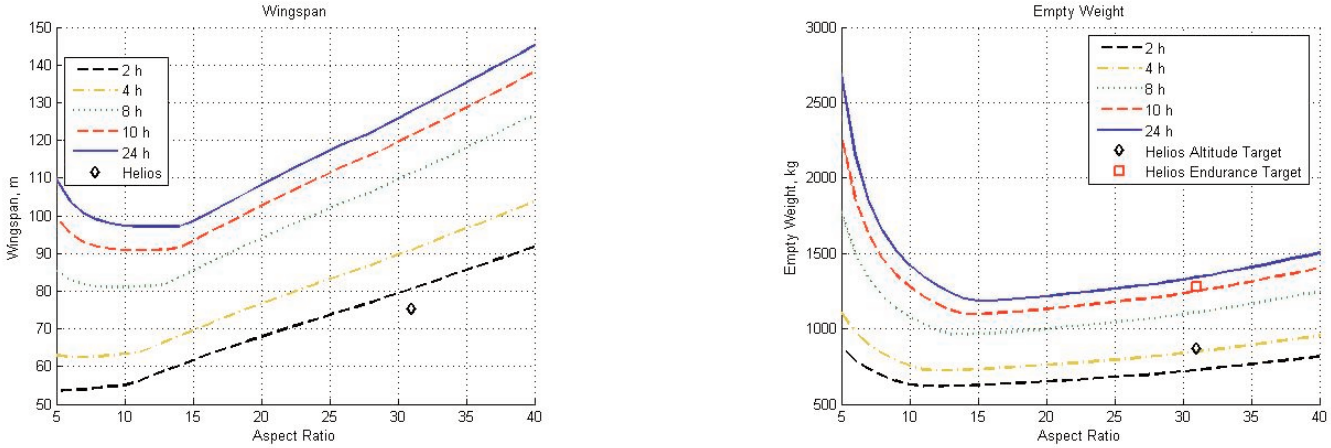



Figure 20. Wingspan and empty weight comparison.

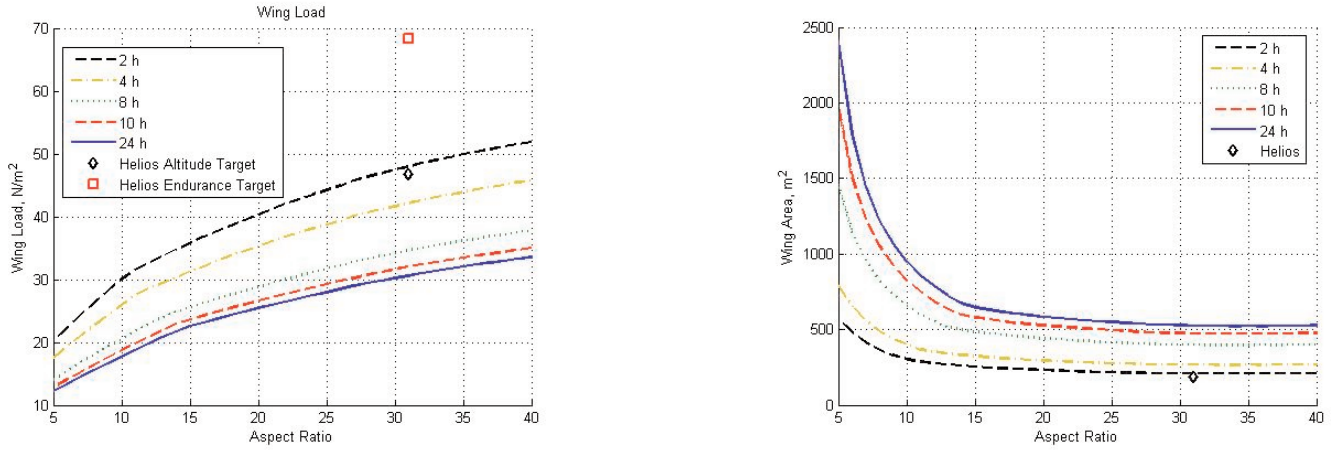



Figure 21. Wing loading and wing area.

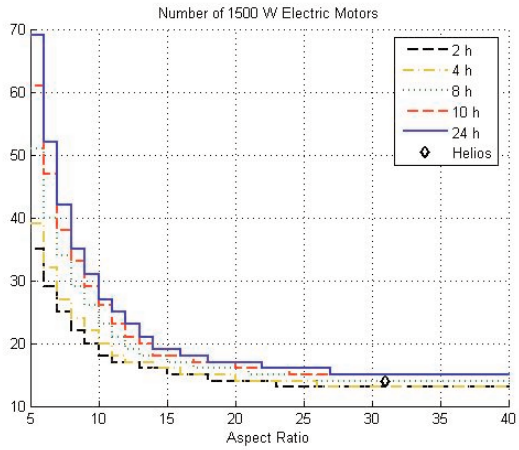



Figure 22. Number of electric motors.

wing loading is lower than Helios wing loading, especially for the maximum endurance flight. This result is also in accordance with the wing area data, and it seems that the Helios wing area is lower than that predicted by the present model in the optimum long endurance flight condition.

A further interesting check of the model is the prediction of the power of the installed motors (Fig. 22). By choosing the same motors of Helios aircraft (1,500watt), the present model predicts the same number of motors (14), hence a global installed power of 21kW.

It should be remarked that these comparisons are affected by some limits as, for example, some lack of data, structural solutions adopted, etc. in spite of these limits, the predictions appear to be coherent.

In the next section, the present mathematical model is applied to compare the efficiencies of the four aforementioned aircraft configurations.

## 8.0 COMPARISON OF CANDIDATE CONFIGURATIONS FOR HALE AIRCRAFT

Figures 21-24 show: a flying wing (such as Helios), a conventional aircraft (wing, fuselage, tail), a twin boom aircraft, and a biplane with vertical bulkheads. The reference conditions are shown in table 8 together with the assumed component efficiencies; in particular, the photovoltaic cells are assumed to be silicon based, with a lower efficiency compared to best available (30%) but also lighter than them.

https://doi.org/10.1017/S0001924000002001 Published online by Cambridge University Press



Figure 23. Flying wing.



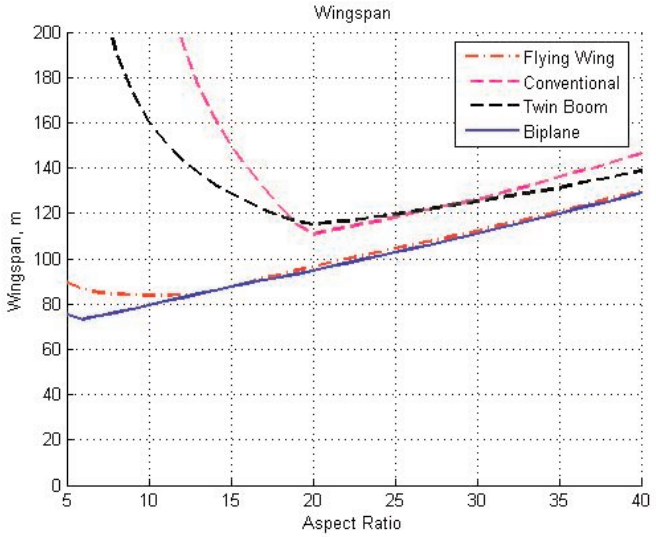
Figure 24. Conventional configuration.



Figure 25. Twin boom.



Figure 26. Reinforced biplane configuration.



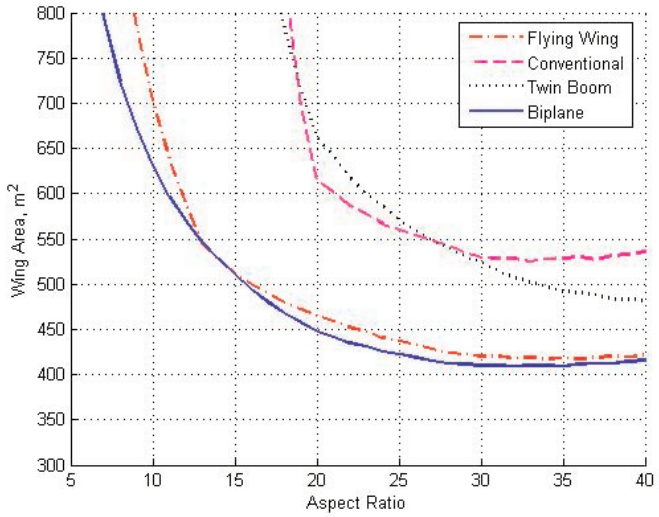




Figure 27. Wingspan and wing area.

**Table 8**
**HALE mission data and component's efficiencies**

| Item | Value |
|---|---|
| Latitude | 44°N |
| Date | 25/06 |
| Altitude | 30km |
| Payload | 300kg |
| Si solar cells efficiency | $\eta = 0{\cdot}19$ |
| Brushless electric motors efficiency | $\eta = 0{\cdot}85$ |
| High altitude optimised propeller efficiency | $\eta = 0{\cdot}8$ |
| Fuel cells efficiency | $\eta = 0{\cdot}5$ |
| Panelled area/wing area | 0·8 |
| $V_{wind}$ | 50ms$^{-1}$ |
| $C_{Lmax}$ | 1 |

The main results obtained are presented in Figs 25–26, and the following parameters are compared: wingspan, area of the lifting surfaces, empty weight and number of electric motors.

As expected, the lowest power consumption configurations have high aspect ratio (more than 30). The most efficient configuration is the biplane with intermediate reinforcements, due to a combination of higher aerodynamic and structural efficiencies; for example, the wingspan is 15% smaller compared to a flying wing with the same surface, and the wing surface is 3-5% smaller compared to a flying wing with the same wingspan. The reduction of the wingspan is important in order to reduce the aeroelastic critical phenomena[9] and also to reduce the required width of the runways. The biplane wings have the same total span so that the aspect ratio of a single wing is double that of a cantilever or flying wing with the same total surface. The result is that, when comparing a biplane and a monoplane with the same lifting surfaces, the bending stiffness of one wing of the biplane is much smaller than that of the equivalent monoplane but in spite of this, the stiffness of the biplane is bigger compared to the monoplane. This conclusion is the result of the static and dynamic calculations of the over-constrained horizontal beams, reinforced with multiple vertical frames. Figure 25 shows that the biplane and the flying wing have the same wing area to fulfil the condition of maximum endurance mission; conventional and twin boom solutions need a larger wing area especially at low aspect ratios. The same conclusions hold as far as the area of the lifting surfaces, empty weight and power installed are concerned. The ratio of structural stiffness and total weight plays the key role in the solutions examined. Figures 27 and 28 show that the maximum tip deflection

https://doi.org/10.1017/S0001924000002001 Published online by Cambridge University Press

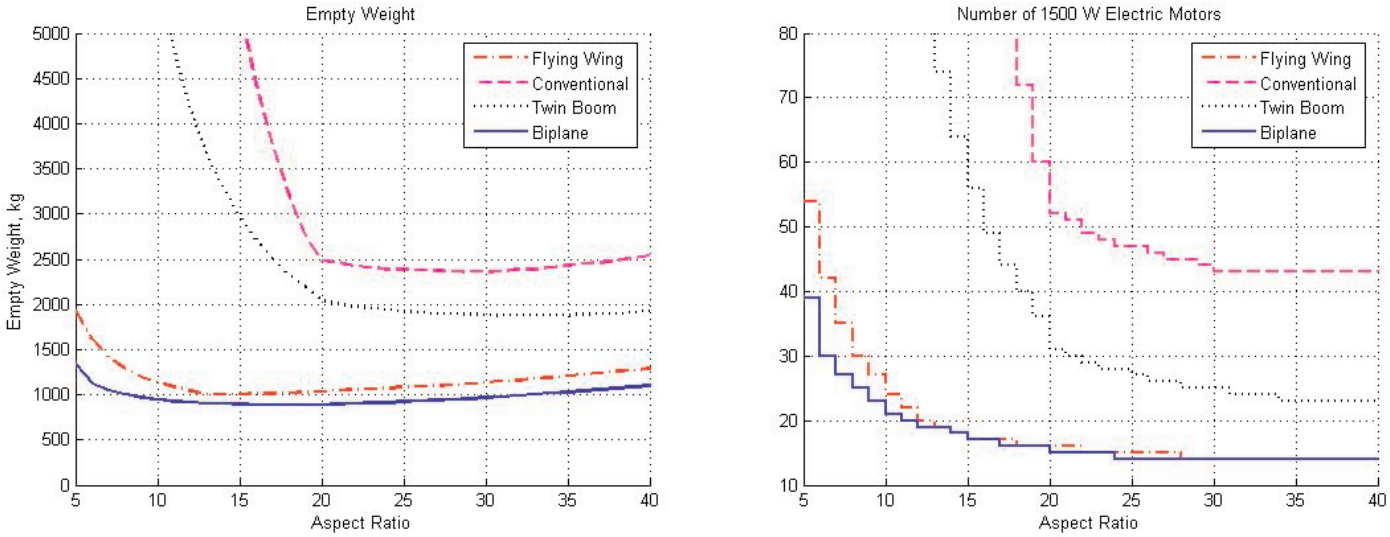



Figure 28. Empty weight and number of electric motors.

**Table 9**
**Derivatives of the wing area**

| DERIVATIVE* | $\partial S_{wing} \Big/ \partial \left(\frac{\eta}{\rho}\right)_{SC}$ | $\partial S_{wing} \Big/ \partial \left(\frac{\eta}{\rho}\right)_{FC}$ | $\partial S_{wing} \Big/ \partial \left(\frac{\eta}{\rho}\right)_{mot}$ |
|---|---|---|---|
| Value | –58·35 | –23·35 | –20·2 |

**Table 10**
**Biplane HALE aircraft data**

| | |
|---|---|
| $AR$ | 25 |
| Wingspan | 71·6m |
| Wing area | 410·2m$^2$ |
| $W_{pay}$ | 330kg |
| $W_{empty}$ | 901·5kg |
| Installed power | 14 × 1,500W |
| $W/S$ | 3kg/m$^2$ |

of a reinforced biplane is about 40% of a cantilever wing, whereas the first natural frequency is 1·6 times higher than the first frequency of the flying wing (see Appendix D for more details).

## 9.0 COST ANALYSIS AND CRITICAL TECHNOLOGIES

The main costs concern the solar cells, the electronics and the control components. The present high efficiency solar cells cost is about 200 €/Watt, for a total of about €6-10m for a single aircraft. As said before, the optimum solar cells are not necessarily the most efficient ones but those having the lower ratio between electrical efficiency and weight. In Table 9, the derivatives of the wing area respect to the ratio are shown, and it appears that the technological progress of the solar cells is more effective than the reduction of fuel cells and motor weights. Figure 29 shows the effect of adding new surfaces to the wing area, under the hypothesis of no weight penalty; this effect is more important when these surfaces are lifting (as, for example, when extracting a panelled flap).

** Calculated for h = 30km, φ = 25 June, biplane configuration.*

## 10.0 AN EXAMPLE OF NEW SOLAR POWERED AIRCRAFT

The proposed theoretical model allows us to predict the effects of changing the design requirements. In this section an example of HALE solar powered aircraft is proposed, in order to meet the mission requirements in Table 8. The aircraft configuration considered here is the reinforced biplane, with the design data shown in Table 10.

Some sketches of the aircraft are reported in the next figures.

A pair of electric motors is positioned at each bulkhead station, with a driving propeller on the front wing and a pushing one on the rear wing. The pitching control can be accomplished either by means of conventional control surfaces (i.e. by elevators) on the rear wing or by elevators on both the wings, rotating in opposition of phase (pitch control with a pure moment) or by differential speed rate control of the upper and lower motors. The yaw control can be obtained by a differential rotation speed control of the motors or by rudders installed at the tip bulkheads or by mixing them together as well. The unusual take off and landing attitude permits a high angle of attack during the take-off phase, with a short take-off run. The take-off run could be performed on a sloped ramp (Fig. 35) as well. The problem of stability of flight of this solution can be easily solved by an appropriate design of the wings, using the experience gained in the design of so called PrandtlPlane aircraft[14].

Figure 34 shows an example of a stable HALE biplane with straight wings. This solution is the result of an aeromechanic optimisation process, involving the integration of a VLM solver[13] associated with an optimiser. The centre of gravity is positioned between the two wings as shown in the above figure. A 53% of the lift is generated by the forward wing, whereas its area is the 33% of the overall lifting area, because of the different twist variations along the span and the presence of a high up-wash on the forward wing and a downwash on the rearward wing. Figure 35 shows the load distributions over the wings. Figure 36 shows the $C_i$ and the $C_{fi}c/C_{ref}$

https://doi.org/10.1017/S0001924000002001 Published online by Cambridge University Press

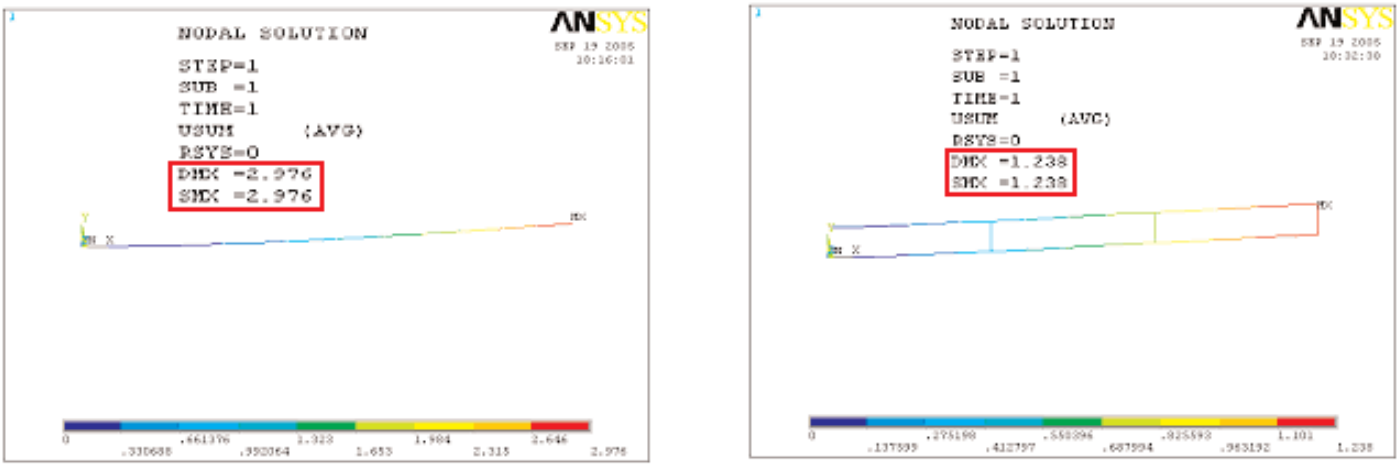



Figure 29. Maximum tip deflection. Cantilever wing (on the left), reinforced biplane (on the right).

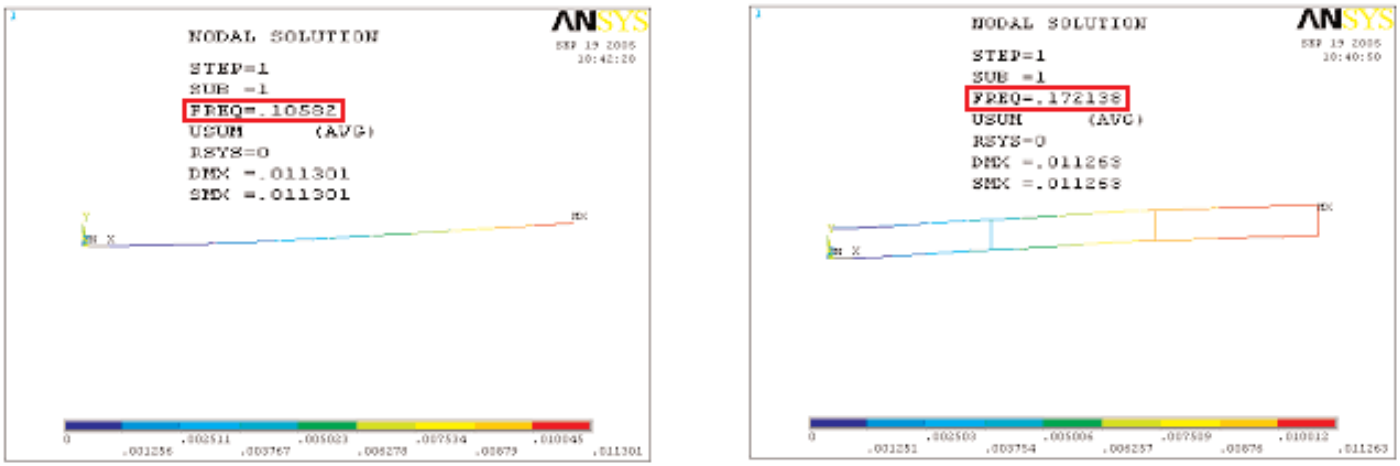



Figure 30. First natural frequency. Cantilever wing (on the left), reinforced biplane (on the right).

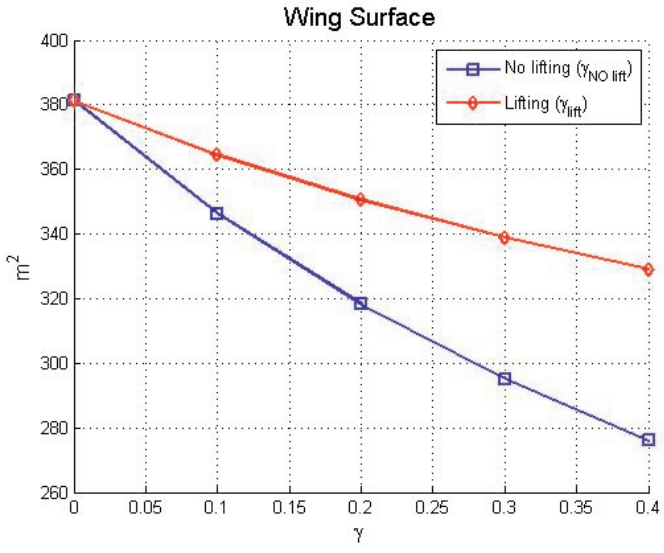



Figure 31. Wing surface *vs* adjunctive deployable panelled surface.

plots calculated in the Trefftz plane.

The lift on the two wings is nearly the same, so that this solution realises the best wing system optimum condition for the induced drag with an Oswald coefficient of 1·015 (this low value is due to the low $h/b$ ratio). The dihedral of the forward wing is 2deg, whereas on the rearward wing is 1deg to guarantee the lateral stability.

## 11.0 CONCLUSIONS

A model for the preliminary design of solar powered high altitude aircraft has been developed. The design can be performed for different operating altitudes, at different latitudes, in different seasons for different payloads and for any aerodynamic configuration. The model has given good results when compared to existing HALE solutions, as NASA solar powered aircraft (Helios), but more investigations need to be performed, particularly for the component weight estimations and the structure optimisation. For HALE aircraft the total required electric power is about 20-25kW and this produces configurations with very large values of photovoltaic panels area and wingspan. Hence, the structural efficiency becomes very important and the optimum configuration combines high values of the structural stiffness to the empty

https://doi.org/10.1017/S0001924000002001 Published online by Cambridge University Press

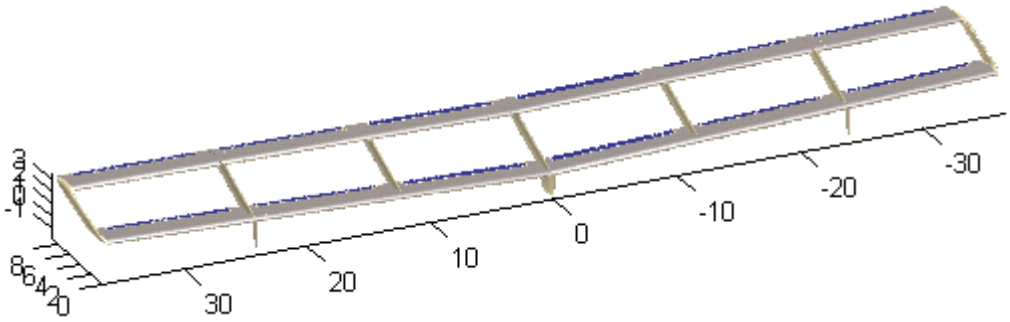



Figure 32. HALE biplane aircraft: isometric view.

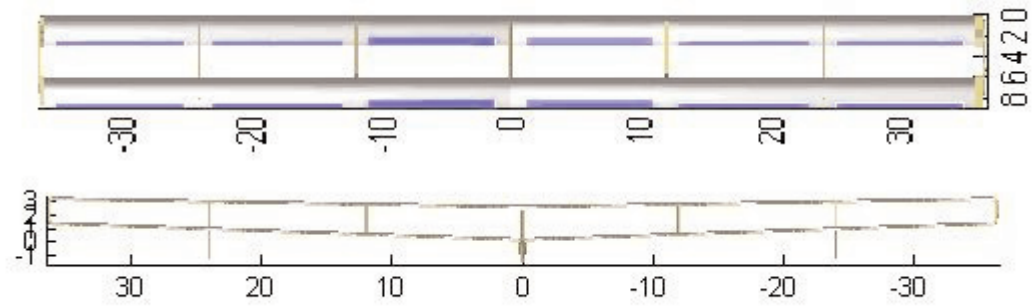



Figure 33. HALE biplane aircraft: top view and front view.

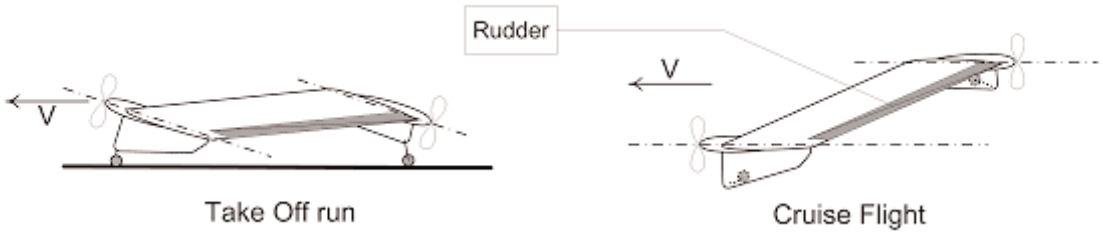



Figure 34. HALE biplane aircraft: take-off and landing position, and (right) during cruise flight (side view).

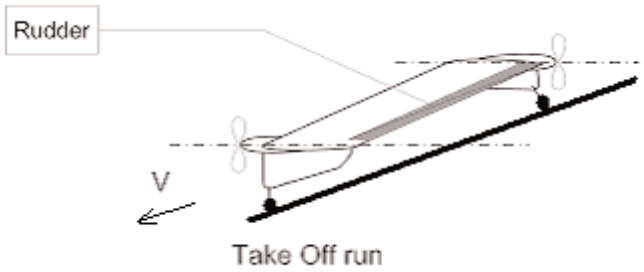



Figure 35. Alternative take-off procedure.

weight ratio, and of the efficiencies of each component.

We have compared four different architectures, and we have shown that a new non-conventional aircraft configuration must be taken in consideration as the best compromise between structural stiffness and energetic efficiency. An example relevant to a biplane configuration with reinforcement bulkheads regularly disposed along the span has been shown. This solution is stiffer than the flying wing and its structural weight can be considered as 80% of the flying wing weight. Moreover, the wingspan is reduced of about 15% compared with the flying wing with same wing surface, and the tip deflection is about 40% of the flying wing with same wingspan and same wing surface: this configuration could avoid the typical aeroelastic

https://doi.org/10.1017/S0001924000002001 Published online by Cambridge University Press

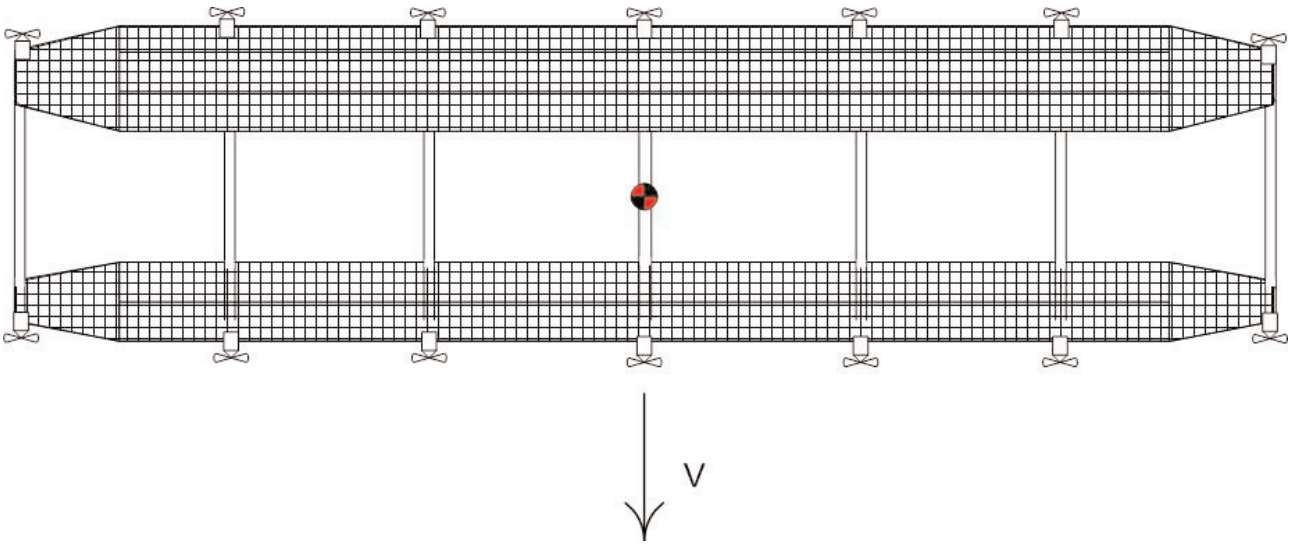



Figure 36. An example of a stable straight wings PrandtlPlane.

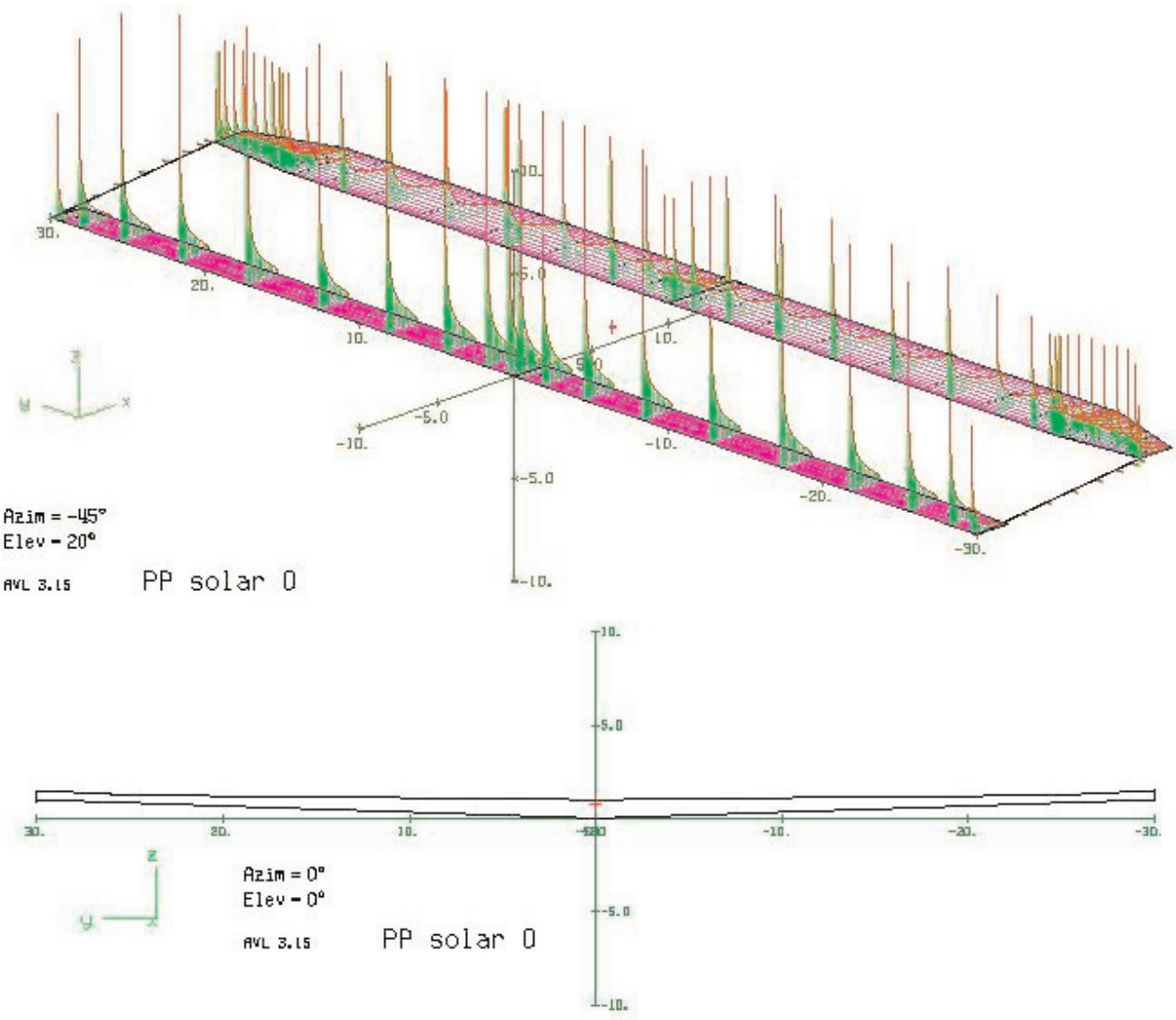



Figure 37. Loads distribution over the wings.

https://doi.org/10.1017/S0001924000002001 Published online by Cambridge University Press

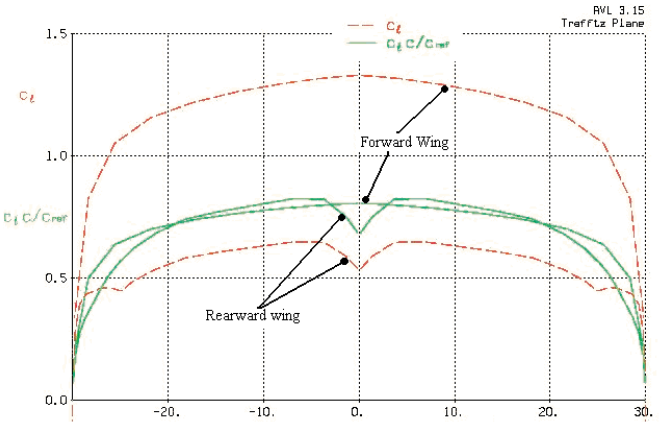



Figure 38. Lift distribution in the Trefftz plane.

problems of high aspect ratio wings.

Technological efforts should be made in the solar cells field (higher value of the efficiency to specific weight ratio) and in the general aircraft layout (use of deployable panelled surfaces for missions at different altitudes and latitudes).

Further improvements in the storage system equipment are needed, especially in terms of specific power or specific energy and on the reliability of the fuel cells plant.

## REFERENCES


1. YOUNGBLOOD, J.W. ET AL Design of long-endurance unmanned airplanes incorporating solar and fuel cell propulsion, 1984, AIAA/SAE/ASME 20th Joint Propulsion Conference.
2. JONES, R.I. The design challenge of high altitude long endurance (HALE) unmanned aircraft, *Aeronaut J*, June 1999, pp 273-280.
3. MACCREADY, P.B. ET AL Sun-powered aircraft design, *J Aircr,* **20**, (6), June 1983 pp 487-493.
4. ROMEO, G. and FRULLA, G. HELIPLAT®: high altitude very-long endurance solar powered UAV for telecommunication and Earth observation applications, *Aeronaut J*, June 2004, pp 277-293.
5. Official Dryden Research Center Site: http://www.dfrc.nasa.gov/Research/Erast/
6. NOLL, T.E. ET AL Investigation of the Helios prototype aircraft mishap, January 2004, www.nasa.gov/pdf/64317main_helios.pdf.
7. COLELLA, N.J. and WENNEKER, G.S. Carnegie Mellon University Pathfinder and the development of solar rechargeable aircraft, July 1994, E&TR, www.llnl.gov/etr/pdfs/07_94.1.pdf.
8. CUFFIE, J.A. and BECKMAN, W.A. *Solar Engineering of Thermal Processes*, 1991, Second edition, John Wiley & Sons.
9. MAYURESH J. PATIL and HODGES, D.H. Nonlinear aeroelasticity and flight dynamics of high-altitude long-endurance aircraft, *J Aircr*, January-February 2001, **38**, (1), pp 88-94.
10. LISSAMAN, P.B.S. and BROWNLOW, L.W. Torsional/flexural response of large span wings to high altitude turbulence, *Aeronaut J*, June 2002, pp 325-335.
11. VENDURA, G.J., MALONE, P. and CRAWFORD, L. A novel, light weight solar array: comparison with conventional systems www.lgarde.com/people/papers/comparison.pdf 2003.
12. MARKEL, ET AL. Energy storage system requirements for hybrid fuel cell vehicles advanced automotive battery, 2003, Conference, Nice, France, 10-13 June 2003, http://www.ctts.nrel.gov/.
13. DRELA, M. AVL 3.14 User Primer, August 2004, MIT Aero & Astro, Harold Youngren, Aerocraft, http://web.mit.edu/drela/Public/web/avl/.
14. FREDIANI, A. The Prandtl Wing, Innovative configurations and advanced concepts for future civil aircraft; 2005, Lecture Series 2005-06, Von Karman Institute, TORENBEEK, E. and DECONINCK, H. (Eds).


## APPENDIX A

The declination δ referred to the *n*-th day of the year can be found from Cooper's equation (1969)[8]:

$$\delta = 23 \cdot 45 \mathrm{Sin}\left(360\frac{284+n}{365}\right) \quad \ldots (71)$$

Useful equations relating the angle-of-incidence, θ, to the other angles are:

$$\mathrm{Cos}\theta = \mathrm{Sin}\delta\mathrm{Sin}\varphi\mathrm{Cos}\beta - \mathrm{Sin}\delta\mathrm{Cos}\varphi\mathrm{Sin}\beta\mathrm{Cos}\gamma + \mathrm{Cos}\delta\mathrm{Cos}\varphi\mathrm{Cos}\beta\mathrm{Cos}\omega + \\ + \mathrm{Cos}\delta\mathrm{Sin}\varphi\mathrm{Sin}\beta\mathrm{Cos}\gamma\mathrm{Cos}\omega + \mathrm{Cos}\delta\mathrm{Sin}\beta\mathrm{Sin}\gamma\mathrm{Sin}\omega \quad \ldots (72)$$

and:

$$\mathrm{Cos}\theta = \mathrm{Cos}\theta_z\mathrm{Cos}\beta + \mathrm{Sin}\theta_z\mathrm{Sin}\beta\mathrm{Cos}\left(\gamma_s - \gamma\right) \quad \ldots (73)$$

Equation (73) can be further simplified under the following assumptions:

The azimuth angle γ is 0° or 180°; this means that the panelled surface is sloped towards South and North respectively:

$$\mathrm{Cos}\theta = \mathrm{Sin}\delta\mathrm{Sin}\varphi\mathrm{Cos}\beta \mp \mathrm{Sin}\delta\mathrm{Cos}\varphi\mathrm{Sin}\beta \quad \ldots (74)$$

$$\vdash \mathrm{Cos}\,\delta\mathrm{Cos}\,\varphi\mathrm{Cos}\,\beta\mathrm{Cos}\,\omega \pm \mathrm{Co}\;s\delta\,\mathrm{Sin}\varphi\,\mathrm{Sin}\beta\,\mathrm{Cos}\omega$$

β = 90° (the panelled surface is set vertically):

$$\mathrm{Cos}\theta = -\mathrm{Sin}\delta\mathrm{Cos}\varphi\mathrm{Cos}\gamma + \mathrm{Cos}\delta\mathrm{Sin}\varphi\mathrm{Sin}\beta\mathrm{Cos}\gamma\mathrm{Cos}\omega \cdot \\ + \mathrm{Cos}\delta\mathrm{Sin}\gamma\mathrm{Sin}\omega \quad \ldots (75)$$

β = 0°, (the panelled surface is set horizontally):

$$\theta_z = \theta$$

$$\mathrm{Cos}\theta_z = \mathrm{Cos}\varphi\mathrm{Cos}\delta\mathrm{Cos}\omega + \mathrm{Sin}\varphi\mathrm{Sin}\delta \quad \ldots (76)$$

$\gamma_s$ is estimated following Braun and Mitchell (1983)[8]:

$$\gamma_s = C_1C_2\gamma'_s + 90C_3\left(1 - C_1C_2\right) \quad \ldots (77)$$

The definitions of $\gamma'_s$, $C_1$, $C_2$, $C_3$ can be found in Ref. 8.

Outside the atmosphere, the radiation on a photovoltaic panel, sloped of an angle β, is:

$$I_0 = I_{SC}\left(1 + 0 \cdot 033\mathrm{Cos}\frac{360n}{365}\right)\mathrm{Cos}\theta_z \quad \ldots (78)$$

If β = 0° using Equation (76), the Equation (78) becomes:

$$I_0 = I_{SC}\left(1 + 0 \cdot 033\mathrm{Cos}\frac{360n}{365}\right)\left(\mathrm{Cos}\varphi\mathrm{Cos}\delta\mathrm{Cos}\omega + \mathrm{Sin}\varphi\mathrm{Sin}\delta\right)$$

## APPENDIX B

**Scattering.** The phenomenon of scattering is due to air molecules, dust molecules and water vapour in the atmosphere; the scattering transmittance can be represented as:

$$\tau_{scatt} = \tau_a\tau_{dust}\tau_w \quad \ldots (79)$$

We assume that the values of the air scattering transmittances are obtained from the Rayleigh theory:

$$\tau_a\left(\lambda\right) = 10^{-\frac{0 \cdot 00384}{\lambda}} \quad \ldots (80)$$

https://doi.org/10.1017/S0001924000002001 Published online by Cambridge University Press

The effect on the transmittance due to dust can be expressed as:

$$\tau_{dust}(\lambda) = 10^{-0{\cdot}00353\lambda^{-0.75}} \quad \ldots (81)$$

According to Moon (1940), water vapour, ozone ($O_3$) and $CO_2$ effects are represented as:

$$\tau_{w}(\lambda) = 10^{-0{\cdot}0075\lambda^{-2}} \quad \ldots (82)$$

Under the following reference conditions:

Atmospheric pressure $p_0$ = 760mm Hg;
Air mass = 1;
Dust concentration: 800 particles/cm$^3$;
Falling water: 20mm.
For different conditions, the following correction holds:

$$\tau_{scatt}(\lambda) = \left[\tau_a^{p/p_0}\tau_{dust}^{d/800}\tau_w^{w/20}\right]^{AM} \quad \ldots (83)$$

where $p$ is the air pressure, $d$ is the dust concentration [particles/cm$^3$]; $w$ is the falling water [mm]; $AM$ is the air mass.

Another approach is to use the Ångström's turbidity equation to predict the dust and water vapour effects on the transmittance:

$$\tau_{d,w} = e^{-\beta\lambda^{-\alpha}AM} \quad \ldots (84)$$

where $\beta$ is the Ångström's turbidity coefficient, varying from 0 (clean atmosphere condition ) to 0·4 (very turbid atmosphere); $\alpha$ depends on the size distribution of the aerosols ($\alpha$ = 1·3 is commonly used).

Using the Ångström's model, the scattering transmittance factor is:

$$\tau_{scatt}(\lambda) = \left[\tau_a^{p/p_0}e^{-\beta\lambda^{-\alpha}}\right]^{AM} \quad \ldots (85)$$

From Equation (84) it follows that the scattering effect is active at lower wavelengths; in particular, according to Rayleigh's law, the scattering transmittance is small when $\lambda > 0{\cdot}6\ \mu m$.

Scattering depends on the pressure (i.e. on the flight altitude) and on the atmospheric conditions (due to the $\beta$ coefficient in the Equation (85), due to $d$ and $w$ in the Equation (83)).

## APPENDIX C: CALCULATION OF THE GEOMETRIC FACTORS

**$\beta_i$ factor for a conventional aircraft**

For a conventional aircraft, the $\beta_i$ factors can be approximately calculated as follows.

**Cylindrical fuselage**:

$$\beta_{fus} = \frac{S_{fus}^{rif}}{S_{wing}} = \frac{2RL}{bc} \quad \ldots (86)$$

For the horizontal tail, using the tail volume definition:

$$\frac{S_{HT}}{S_{wing}} = \frac{V_{HT}\bar{c}}{L_{HT}} \quad \ldots (87)$$

where $V_{HT}$ is the horizontal tail volume and $L_{HT}$ is the distance between the aerodynamic centre of the horizontal tail and the aerodynamic centre of the wing.

**Vertical tail:**

$$\frac{S_{VT}}{S_{wing}} = \frac{V_{VT}b}{L_{VT}} \quad \ldots (88)$$

where $V_{VT}$ is the vertical tail volume and $L_{VT}$ is the distance between the aerodynamic centre of the fin and the aerodynamic centre of the wing. Because we have chosen the surface projected on the horizontal plane as reference area, we must lead back to this last one the vertical tail surface. The following expressions hold:

$S_{VT} = c_{VT}\,b_{VT}$: vertical tail area; with $c_{VT}$: vertical tail chord and $b_{VT}$ vertical tail length;

$S_{VT}^{rif} = c_{VT}{}^2\,(t/c)_{VT} = \left(\frac{S_{VT}}{b_{VT}}\right)^2 (t/c)_{VT}$ vertical tail reference area, i.e. vertical tail area projected onto the horizontal plane; this relation is true for a straight rectangular wing;

$AR_{VT} = \frac{b_{VT}{}^2}{S_{VT}}$ : vertical tail aspect ratio, from which;

finally we get:

$$S_{VT}^{rif} = \frac{S_{VT}}{AR_{VT}}(t/c)_{VT} \Rightarrow \frac{S_{VT}^{rif}}{S_{wing}} = \frac{S_{VT}}{S_{wing}}\frac{(t/c)_{VT}}{AR_{VT}} = \frac{V_{VT}b}{L_{VT}}\frac{(t/c)_{VT}}{AR_{VT}} \quad \ldots (89)$$

From the previous relations, it follows that we must know the tail volumes and the position of the aircraft's centre of mass to obtain the $\beta_i$ coefficients. We can get them from statistical data for sail planes with two booms fins[1]. Recommended values are:

$$\frac{S_{HT}}{S_{wing}} = 0{\cdot}31 \quad \ldots (90)$$

$$\frac{S_{VT}}{S_{wing}} = 0{\cdot}1 \Rightarrow \frac{S_{VT}^{rif}}{S_{wing}} = \frac{S_{VT}}{S_{wing}}\frac{(t/c)_{VT}}{AR_{VT}} \quad \ldots (91)$$

These data can be obtained by statistical data for commercial aircrafts and with the further assumption of 'square aircraft', that is $b/2 \approx L_F$.

With these hypotheses:

$V_{HT} = 1$ ; (typical value for commercial aircraft)
$V_{HT} = 0{\cdot}09$; (typical value for commercial aircraft)
$L_{HT} = L_{VT} = 0{\cdot}5\ L_{fus} \approx b/4$; (typical value for commercial aircraft)

$$\beta_{fus} = \frac{S_{fus}^{rif}}{S_{wing}} = \frac{2RL_F}{bc} \approx R/c \quad \ldots (92)$$

$$\frac{S_{HT}}{S_{wing}} = \frac{V_{HT}\bar{c}}{L_{HT}} \approx \frac{4}{AR} \quad \ldots (93)$$

$$\frac{S_{VT}^{rif}}{S_{wing}} = \frac{V_{VT}b}{L_{VT}}\frac{(t/c)_{VT}}{AR_{VT}} \approx \frac{0{\cdot}09}{0{\cdot}25}\frac{(t/c)_{VT}}{AR_{VT}} = 0{\cdot}36\frac{(t/c)_{VT}}{AR_{VT}} \quad \ldots (94)$$

**$\alpha_{VT}$ for a vertical wing**

When the wing is vertical (like a fin), the reference area is the area inside the root airfoil

$$\alpha_{VT} = \frac{S_{VT}^{b}}{S_{VT}^{rif}} \cong \frac{2S_{VT}}{S_{VT}^{rif}} = \frac{2S_{VT}}{2\frac{S_{VT}}{AR_{VT}}(t/c)_{VT}} = \frac{AR_{VT}}{(t/c)_{VT}} \quad \ldots (95)$$

**ß$_{bulk}$ for a biplane**

Assuming the geometry as in the Fig. 39:

The following relations hold:

$S_p = c_{ph}$ bulk lateral surface $\quad \ldots (96)$

https://doi.org/10.1017/S0001924000002001 Published online by Cambridge University Press

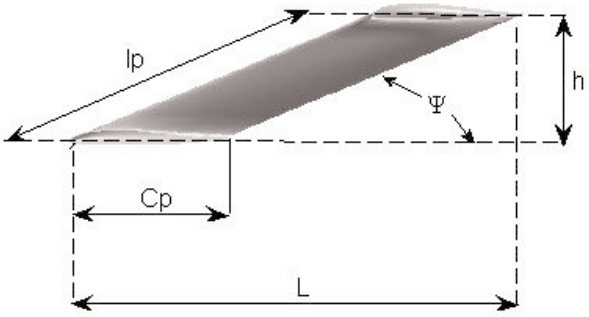



Figure 39. Bulkhead geometry.

$S_p^{rif} = (t/c)_p c_p L$ reference bulk area . . . (97)

$$L = c_p + \frac{h}{tg\psi} \quad \ldots (98)$$

$$tg\psi = \frac{h}{L - c_p} \quad \ldots (99)$$

$$\beta_p = \frac{S_p^{rif}}{S_{wing}} = \frac{(t/c)_p c_p L}{S_{wing}} = \frac{(t/c)_p c_p^2 \left(1 + \frac{h/c_p}{tg\psi}\right)}{S_{wing}} = \frac{(t/c)_p c_p^2 \left(1 + \frac{l_p}{c_p}\mathrm{Cos}\psi\right)}{S_{wing}} \quad \ldots (100)$$

Assuming the wing chord equal to the bulk chord ($c = c_p$):

$$\beta_p = \frac{(t/c)_p \left(1 + \frac{h/c}{tg\psi}\right)}{AR_{wing}} = \frac{(t/c)_p \left(1 + \frac{AR_p}{tg\psi}\right)}{AR_{wing}} \quad \ldots (101)$$

where $AR_p = \frac{h}{c_p}$.

If $L = 2c_p$, we get:

$$\beta_p = 2\frac{(t/c)_p}{AR_{wing}} \quad \ldots (102)$$

**$a_{bulk}$ factor for a biplane**

The following relationships hold:

$S_{bulk}^b \approx 2S_{bulk} = 2c_p h$ bulk wetted area . . . (103)

$S_{bulk}^{rif} = (t/c)_p c_p L$ reference bulk area . . . (104)

hence:

$$\alpha_{bulk} = \frac{S_{bulk}^b}{S_{bulk}^{rif}} = \frac{2h}{(t/c)_p L} \quad \ldots (105)$$

from which:

$$\alpha_{bulk} = \frac{2h}{(t/c)_p c_p \left(1 + \frac{h/c_p}{tg\psi}\right)} = \frac{2h}{(t/c)_p c_p \left(1 + \frac{AR_p/2}{tg\psi}\right)} \quad \ldots (106)$$

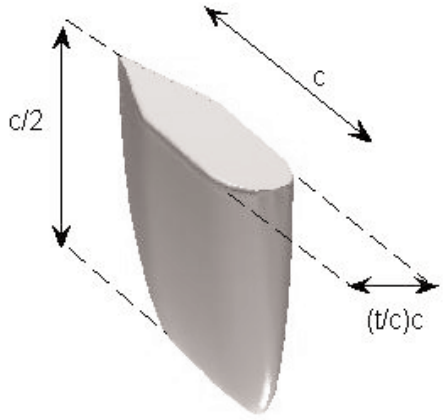



Figure 40. Pod geometry.

If $L = 2c_p$,, we get:

$$\alpha_{bulk} = \frac{h/c_p}{(t/c)_p} = \frac{h}{b}\frac{AR_{wing}}{(t/c)_p} \quad \ldots (107)$$

The bulk rate to the wetted area is:

$$NP\alpha_{bulk}\beta_{bulk} = NP\frac{h}{b}\frac{AR_{wing}}{(t/c)_p}2\frac{(t/c)_p}{AR_{wing}} = 2NP\frac{h}{b} \quad \ldots (108)$$

**$\alpha_{pod}$ and $\beta_{pod}$ factors**

Let $N_{pod}$ the number of pods from previous NASA prototypes (Pathfinder, Centurion and Helios) we get the following law $N_{pod} = AR/6$ and the relations between the dimensions as in Fig. 40.

It follows:

$$S_{pod}^b \approx 2S_{pod} = 2c_{pod}\frac{c_{pod}}{2} = c_{pod}^2 \text{ pod wetted area} \quad \ldots (109)$$

$$S_{pod}^{rif} = (t/c)_{pod} c_{pod} c_{pod} = (t/c)_{pod} c_{pod}^2 \text{ pod reference area} \quad \ldots (110)$$

then:

$$\alpha_{pod} = \frac{S_{pod}^b}{S_{pod}^{rif}} = \frac{1}{(t/c)_{pod}} \quad \ldots (111)$$

For the $\beta_{pod}$ factor, from its definition it follows:

$$\beta_{pod} = \frac{S_{pod}^{rif}}{S_{wing}} = \frac{(t/c)_{pod} c_{pod}^2}{bc} \text{ and, assuming } c_{pod} = c, \text{ we get:}$$

$$\beta_{pod} = \frac{S_{pod}^{rif}}{S_{wing}} = \frac{(t/c)_{pod} c}{b} \quad \ldots (112)$$

The wetted area increase due to pods is:

$\alpha_{pod}\beta_{pod} = 1/AR$ for one pod;

$N_{pod}\alpha_{pod}\beta_{pod} = \frac{1}{6}$ for $NP$ pods. . . . (113)

https://doi.org/10.1017/S0001924000002001 Published online by Cambridge University Press

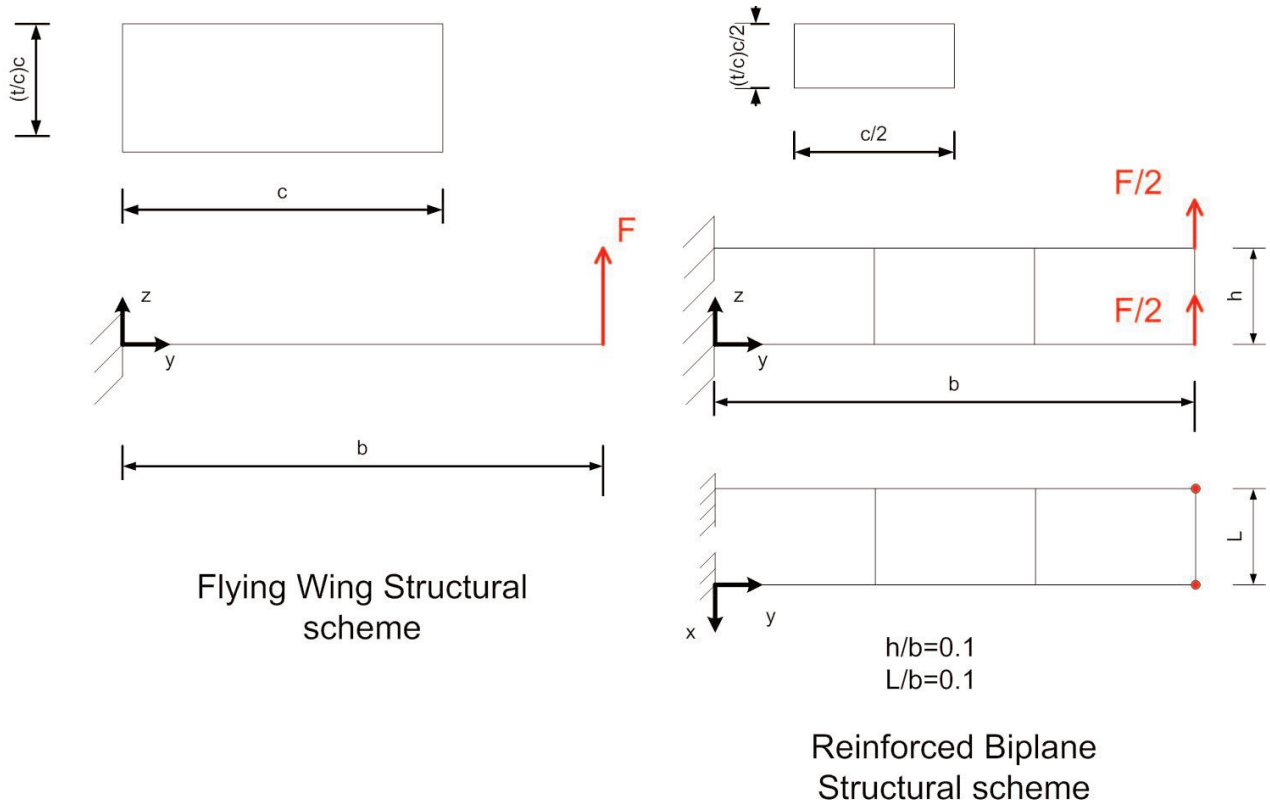



Figure 41. Structural scheme.

## APPENDIX D: STRUCTURAL MODEL

Let us consider a cantilever wing with a vertical force at a tip (Fig. 41, left) and a biplane with reinforcement bulkheads as shown in Fig. 41 (right). The moments of inertia are considered constant along the wingspan.

The vertical tip displacement of the cantilever wing is given by:

$$v_{FW} = \frac{Fb^3}{3EI} \qquad \ldots (114)$$

The expression for the biplane is more complicated and a closed form will not be given here but a FEM analysis has been performed instead.

https://doi.org/10.1017/S0001924000002001 Published online by Cambridge University Press